Rijksdienst voor Ondernemend Nederland

# Seizoensopslag van zonnewarmte door magnesiumsulfaat heptahydraat

EOS-LT Waels

Datum Maart 2009

ECN, TU Eindhoven

In opdracht van SenterNovem (nu Rijksdienst voor Ondernemend Nederland)

Publicatienr RVO-159-1501/RP-DUZA
www.rvo.nl
Dit rapport is tot stand gekomen in opdracht van het ministerie van Economische Zaken.

Confidential


# Characterization of magnesium sulfate as thermochemical material for seasonal heat storage

**V. M. van Essen, H.A. Zondag, L.P.J. Bleijendaal, R. Schuitema, M. Bakker, W.G.J. van Helden**

Energy in the Built Environment Unit, Energy research Center of the Netherlands (ECN), 1755 ZG Petten, the Netherlands

**Z. He**

Department of Mechanical Engineering, Eindhoven University of Technology (TU/e), 5600 MB Eindhoven, the Netherlands

ECN-0--08-000 MARCH 2009

# Acknowledgement/Preface

In this report the results of the characterization experiments on magnesium sulfate (MgSO4.7H2O) are presented. The experimental work was performed together with Eindhoven University of Technology within the WAELS (Woningen als Energieleverend Systeem; House As Energy Supplying System).

This project has received financial support from the Dutch Ministry of Economic Affairs by means of the EOS support scheme. The work on thermo chemical heat storage is part of the long-term work at ECN on compact storage technologies.

# Contents

## List of tables



## List of figures

## Summary

Magnesium sulfate hepta hydrate ($MgSO_4.7H_2O$) was studied as possible thermochemical material for seasonal storage of solar heat. Both hydration and dehydration were investigated and it was found that the material can be used to store almost 10 times more energy than water of the same volume using a solar collector (vacuum tube). The amount of stored solar heat that can be released by the material turned out to be strongly dependent on the water vapor pressure and temperature. Under practical conditions ($P_{H2O}$=12 mbar and T=50°C), the material was not able to release all the stored heat. Despite this problem, valuable information on the dehydration and hydration behavior of $MgSO_4.7H_2O$ was acquired and the characterization procedure will also be used for future characterization of other salt hydrates for thermochemical materials

# Introduction

Today the spotlight in the world is on the increasing demand on sustainable and renewable energy sources. Solar energy is one of the most important sources, which could provide durable heat for various applications [1]. However, it is most effective in summer and not in winter when the available solar energy is not enough to meet the heating demand. A solar heat storage is necessary to accommodate the difference in time between energy production and energy demand. There are three ways for solar energy storage: sensible heat, phase change reaction, and thermochemical reaction [2]. The storage using thermochemical materials shows more advantages for practical applications: thermochemical materials have the highest storage capacity among all the storage media and there is no heat loss associated with thermochemical storage.

A previous study at ECN [2] indicated magnesium sulfate heptahydrate ($MgSO_4.7H_2O$) as potentially interesting thermochemical storage material using the following reversible reaction:

$$MgSO_4.7H_2O(s) + \text{heat} \Leftrightarrow MgSO_4(s) + 7H_2O\ (g) \qquad (R.1)$$

The theoretical storage density of $MgSO_4.7H_2O$ is 2.8 GJ/m$^3$ at temperature level of 122°C, which offers a more compact way of storing energy for the same volume in comparison to water (0.25 GJ/m$^3$ at temperature range of 25-85°C). It also means that the material can be dehydrated using a solar collector, which is assumed to realize a maximum temperature of 150°C. In addition to the high storage density, $MgSO_4.7H_2O$ is cheap, non-toxic and non-corrosive. For these reasons, $MgSO_4.7H_2O$ is studied at ECN as possible thermochemical material for compact (seasonal) heat storage within the Dutch WAELS project.

Epsomite ($MgSO_4.7H_2O$), hexahydrate ($MgSO_4.6H_2O$) and kieserite ($MgSO_4.H_2O$) are the dominant natural occurring magnesium sulfates on earth. Reaction R.1 suggests a single step dehydration process, but the actual dehydration is believed to proceed in discrete steps [3-5]. During the dehydration of Epsomite several other (unstable) members of the magnesium sulfate-water system have been identified such as $MgSO_4.5H_2O$ (Pentahydrate), $MgSO_4.4H_2O$ (Leonhardtite), $MgSO_4.3H_2O$, $MgSO_4.2H_2O$ (Sanderite), $MgSO_4.1{,}5H_2O$ and $MgSO_4.0{,}5H_2O$ [5-9].
Many experiments have indicated that the first step in the dehydration of $MgSO_4.7H_2O$ results in the loss of one water molecule [3, 6, 10]. However, this well-defined transition is an exception in the description of the magnesium-water system: the available literature on dehydration of $MgSO_4.7H_2O$ shows a disagreement on which intermediates are formed during dehydration of $MgSO_4.6H_2O$. For example, Ruiz et al [3] suggests that the dehydration proceeds via crystalline $MgSO_4.6H_2O$, which dehydrates via an amorphous (unknown) intermediate state until crystalline amorphous $MgSO_4$ is formed. Emons [5] identifies $MgSO_4.3H_2O$ and $MgSO_4.2H_2O$ as intermediates during the dehydration of $MgSO_4.7H_2O$, while other investigators [6-9] observe the formation of other intermediates such as Pentahydrate and Leonhardtite. To investigate the potential of $MgSO_4.7H_2O$ as thermochemical material, it is necessary to know which reactions are taking place during the dehydration and at what temperatures.
Compared to dehydration, less is known about the hydration processes within the $MgSO_4$-water system. A recent investigation on hydration behavior of magnesium sulfate [11, 12] indicates that the hydration within $MgSO_4$-water system is complex and depends strongly on the relative humidity and temperature. The authors found that other hydrates than $MgSO_4.7H_2O$, $MgSO_4.6H_2O$ and $MgSO_4.H_2O$ can be formed after hydration. In particular, $MgSO_4.5H_2O$ and an unknown $MgSO_4.2{,}4H_2O$ was identified as a stable product after hydration. It was also found that $MgSO_4.H_2O$ could persist over a large temperature and relative humidity range and can only be converted to $MgSO_4.6H_2O$ or $MgSO_4.7H_2O$ at a high relative humidity (>55% at 25°C).
In a future thermochemical heat storage application, a bore hole at an average temperature of 10°C could be used to evaporate the stored water. This means that a maximum (saturation) wa-

ter vapor pressure of 1.3 kPa is available during hydration. The water vapor will react with the dehydrated salt to retrieve the stored solar heat (see also [R.1]). The released heat will be used for space heating, which means that the hydration should take place at the required temperature for space heating: T≥40°C. At these temperatures a water vapor pressure of 1.3 kPa corresponds to a relative humidity ≤ 17%. In this report we investigate if dehydrated magnesium sulfate is able to take up water and release heat under the above stated conditions. Since the expected life-time of thermal heat storage systems is 20 years, it also means that the material should be able to perform several cycles (hydration-dehydration). Therefore the capacity to store and release heat after several cycles (=cyclability) is also investigated for magnesium sulfate.
In summary, in this report we evaluate $MgSO_4.7H_2O$ as potential thermochemical material by investigating the dehydration and dehydration behavior of magnesium sulfate anew. This study not only provides insight into the potential of $MgSO_4.7H_2O$ as thermochemical material, but will also provide a blue-print for characterization of other potential thermochemical materials.

# 1. Material and methods

In this chapter we will discuss the material and methods which were used for characterization of $MgSO_4.7H_2O$.

## 1.1 Material

Initial characterization experiments [13] were performed using magnesium sulfate heptahydrate (Merck B.V. Benelux, CAS 10034-99-8, GR for analysis, 99.5 % pure). Experiments were also conducted using magnesium sulfate heptahydrate from VWR BDH Prolabo (CAS 10034-99-8, NORMAPUR, 99.5% pure). Here, we will refer to these materials as 'Merck' and 'VWR', respectively.
The powder material from both Merck and VWR were analyzed and are discussed in this report. The material was sieved using a Fritsch vibratory shaker and the sieves of 20, 38, 106, 200 and 500 μm to obtain the powders with different particle size ranges. A particle diameter ranging from 38 to 100 μm was used as reference.

## 1.2 Methods

### 1.2.1 Thermal analysis

Thermal analysis was performed to obtain information on the dehydration and hydration processes in the magnesium sulfate-water system. The goal was to determine the dehydration and hydration reactions, at which temperatures these reactions occur and to determine the heat of reaction. The experiments described here, were performed at ECN and at Netzsch Application Laboratory (Selb, Germany).
The experiments at ECN were performed on a Netzsch STA (TG-DSC) 409 PC Luxx apparatus. For verification, a Netzsch DSC 204 F1 Phoenix apparatus was used for more accurate DSC measurements. Both machines were calibrated prior to the measurements. The sample pans were made of aluminum oxide and were used without lid. The sample mass ranges from 5 to 50 mg, where 10 mg sample mass were used as reference. The experiments were performed in a nitrogen-water vapor atmosphere unless stated otherwise. The nitrogen purge gas (60 ml/min) was saturated with water vapor using a bubble flask and mixed in the oven with nitrogen protective gas (total flow rate of 80 ml/min). The humidity of the gas mixture was measured at the exit of the Netzsch STA 409 PC Luxx apparatus using a dew point meter (Michell Optidew) and found to be ~40% at 25°C ($P_{H2O}$=1.3 kPa). However, the local humidity at the sample could not be determined and therefore a $P_{H2O}$=1.3 kPa was initially assumed near the surface of the sample.
To verify the experiments performed at ECN, a set of experiments was performed at Netzsch Application Laboratory. These experiments were performed on a Netzsch STA (TG-DSC) 409 PG Luxx apparatus equipped with a water vapor furnace capable of operation between 25°C to 1300 °C. Heating rates of up to 50 K/min can be employed and the digital resolution of the balance is 2 μg/digit. The vacuum tight system is connected to a water vapor pressure control system, which allows performing experiments under moisturized nitrogen atmosphere with predefined relative humidity (accuracy of 1%). The experiments were performed using platinum crucibles with pierced lids and a sample mass of ~10 mg. A nitrogen-water vapor atmosphere of R.H. = 40% at 25°C and R.H. = 50% at 30°C were used during the experiments.

### 1.2.2 X-ray powder diffraction

Information on the crystal structure and the different hydrates of magnesium sulfate before, during and after dehydration and hydration was acquired using X-ray powder diffraction. The X-

ray diffraction patterns were collected using a Bruker D8 Advance with MRI oven with Cu KA1+KA2 = 1.5418 Å radiation. Typical runs were conducted from 10° to 40° 2θ using 0.02° step with a time step of 2 seconds. The experimental diffraction patterns were compared to known patterns of magnesium sulfate hydrates [14]. Samples of 150 mg were placed on a platinum grid inside a nitrogen and water vapor atmosphere ($P_{H2O}$ = 2.7 kPa or saturation pressure at 22°C unless stated otherwise). The temperature was increased during dehydration from 25°C to 300°C using a heating rate of 1°C/min and held constant at 25°C during hydration experiments. Diffraction patterns were recorded at temperatures where TG curve indicated a change in composition.

### 1.2.3 Scanning electron microscope with energy-dispersive X-ray spectroscopy (SEM-EDX)

Micro structural changes such as crack formation on a grain level were observed using a JEOL JSM 6330F scanning electron microscope (SEM). The SEM pictures were taken under vacuum conditions, which could initiate further or partial dehydration of the sample. The samples were placed on carbon tape and mounted on a bronze stub. In order to improve the quality of the SEM picture, the samples were platinum coated in a sputter to enhancing the conductivity of the material. The platinum coated samples were viewed under low-pressure $10^{-6}$-$10^{-7}$ mbar at magnifications ranging from 50 to 1500x in the SEM. The beam accelerator voltage was set between 5-15kV.

The SEM was also equipped with element analysis equipment. Here, the element composition of a sample was performed using energy dispersive X-ray spectroscopy (EDX). Here too, the sample is coated with a platinum layer and examined at low pressure ($10^{-6}$-$10^{-7}$ mbar)

### 1.2.4 Particle size distribution measurements

The effect of hydration and dehydration on the particle size distribution was investigated using a Malvern Master 2000. This apparatus is capable of measuring materials in the range of 0.02 μm to 2000 μm using laser diffraction measurement principle (Mie scattering). During the laser diffraction measurements, a suspension of magnesium sulfate and ethanol is flown through a flow cell. To prevent that the magnesium sulfate particles stick together, the suspension is shaken using ultrasound.

# 2. Results and discussion

## 2.1 Experiments performed at ECN

In this section the experiments which were performed at ECN are discussed. These experiments include XRD, STA, DSC, SEM-EDX and particle size distribution measurements. As mentioned above, the STA and (separate) DSC measurements were performed under nitrogen – water vapor atmosphere with an estimated $P_{H2O}$=1.3 kPa at 25°C near the sample surface.

### 2.1.1 Composition of starting material

Several sources indicated [3, 10, 14] that $MgSO_4.7H_2O$ can already convert to $MgSO_4.6H_2O$ at ambient conditions[A] and RH=42-55 %. Therefore it is possible that the composition of the starting material consist of both $MgSO_4.7H_2O$ and $MgSO_4.6H_2O$. For this reason XRD diffraction patterns at 22°C ($P_{H2O}$=2.7 kPa) were taken of the starting material from both Merck and VWR. Figure 1 shows the results of these measurements:

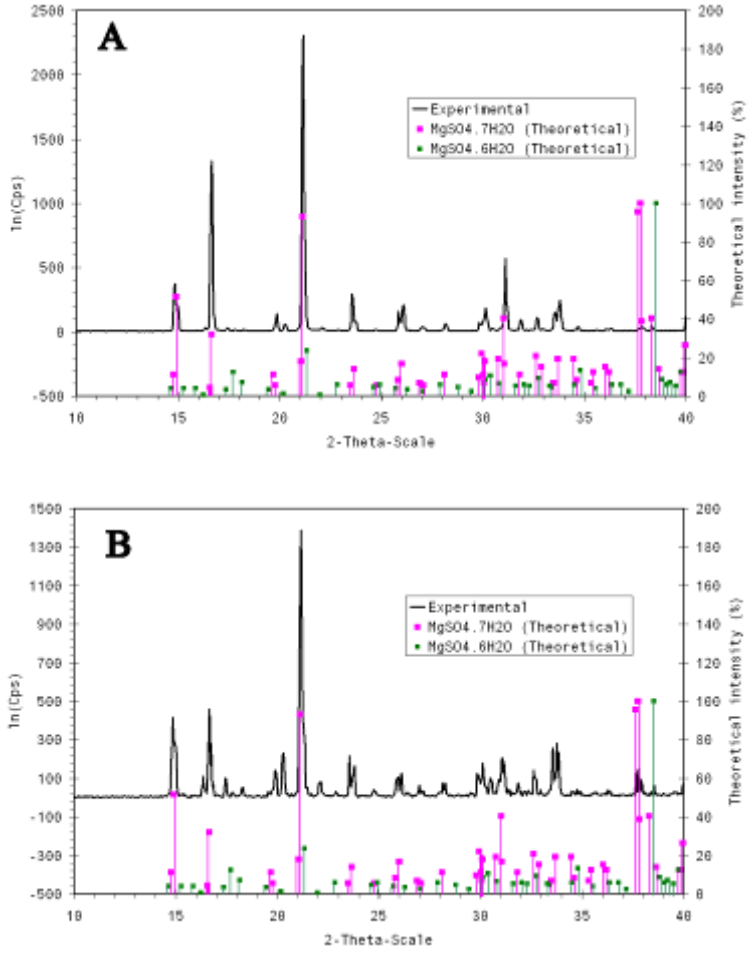


Figure 1: Experimental X-ray diffraction patterns at 22°C ($P_{H2O}$=2.7 kPa) for starting material supplied by A. VWR, B. Merck. Purple bars denote $MgSO_4.7H_2O$ and green bars denote $MgSO_4.6H_2O$ theoretical X-ray diffraction patterns.

[A] Ambient conditions are stated as T=298 K and P=1 atm

The X-ray diffraction pattern for material from VWR corresponds very well with the theoretical X-ray diffraction pattern for $MgSO_4.7H_2O$. The X-ray diffraction pattern for material from Merck shows peaks which correspond with the theoretical X-ray diffraction pattern for both $MgSO_4.6H_2O$ and $MgSO_4.7H_2O$, which indicated that the Merck supplied material is a mixture of $MgSO_4.6H_2O$ and $MgSO_4.7H_2O$.The reason for the difference between the powder materials of the two suppliers is aging of the material: at the time of the measurements, Merck's $MgSO_4.7H_2O$ was ordered more than one year ago and was therefore longer exposed to room conditions, whereas the material from VWR was less than one month old

The results in Figure 1 show that the maximum intensity of some peaks for the material from VWR are different than those for the material from Merck. The ratio between the maximum intensities is determined by the position of the atoms within the crystal structure. For example, ratio of the intensity for the peak at 16.5 and 20 2-theta is different for the two materials. This indicates that the position of the atoms within the crystal structure of material from VWR is different than those for material at Merck. This difference is possibly caused by stress within the crystal structure. It should be noted that the (orthorhombic) crystal structure of $MgSO_4.7H_2O$ remains intact for both materials.

EDX experiments were performed on the starting material from VWR and Merck. The goal of this experiment was to find out if the material was polluted. The results (see Appendix A) indicate that both materials consists of equal amounts of magnesium, sulfide and oxygen atoms (hydrogen cannot be detected using EDX). It means that the chemical composition of the material can be considered identical. The chemical composition of the material was calculated based on the EDX results and it was found that the material consists of $MgSO_4.H_2O$. This results seems to be contradicting the results from the X-ray analysis (see Figure 1), but one should be aware of the fact that a very low pressure was applied during the EDX experiments which causes the material to dehydrated. Apparently, $MgSO_4.H_2O$ is formed during the dehydration of $MgSO_4.7H_2O$. In the next section the dehydration of $MgSO_4.7H_2O$ is studied in more detail.

### 2.1.2 Dehydration of magnesium sulfate hepta hydrate ($MgSO_4.7H_2O$)

In this section the dehydration of magnesium sulfate hepta hydrate is discussed based on the experimental results from TG-DSC and X-ray diffraction measurements. The focus will be mainly on which intermediates are formed during dehydration and the dehydration reactions that are taking place.

#### 2.1.2.1 Thermal analysis: dehydration of magnesium sulfate

Figure 2 shows TG dehydration curves for magnesium sulfate supplied by Merck and VWR:

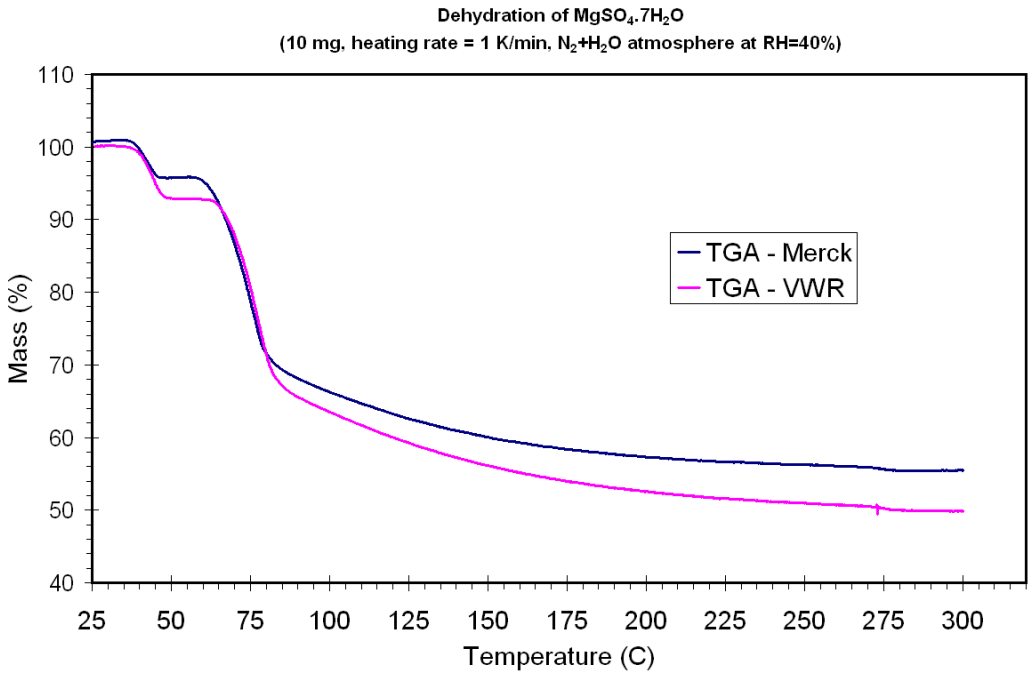


Figure 2: Experimental TG curves as function of temperature of dehydration of $MgSO_4.7H_20$: Comparison between Merck and VWR powder material (particle size = 38-106 μm)

The difference between the TG dehydration curves is a result from the fact that a large part of $MgSO_4.7H_2O$ is already converted to $MgSO_4.6H_2O$ in the starting material supplied by Merck, whereas the powder material supplied by VWR consists of $MgSO_4.7H_2O$ (see above). The difference in dehydration between the two powders (VWR and Merck) is only the composition of the starting material; therefore we will discuss the dehydration of $MgSO_4.7H_2O$ without mentioning the specific manufacturer.

Figure 3 shows two DSC curves for dehydration of $MgSO_4.7H_2O$:

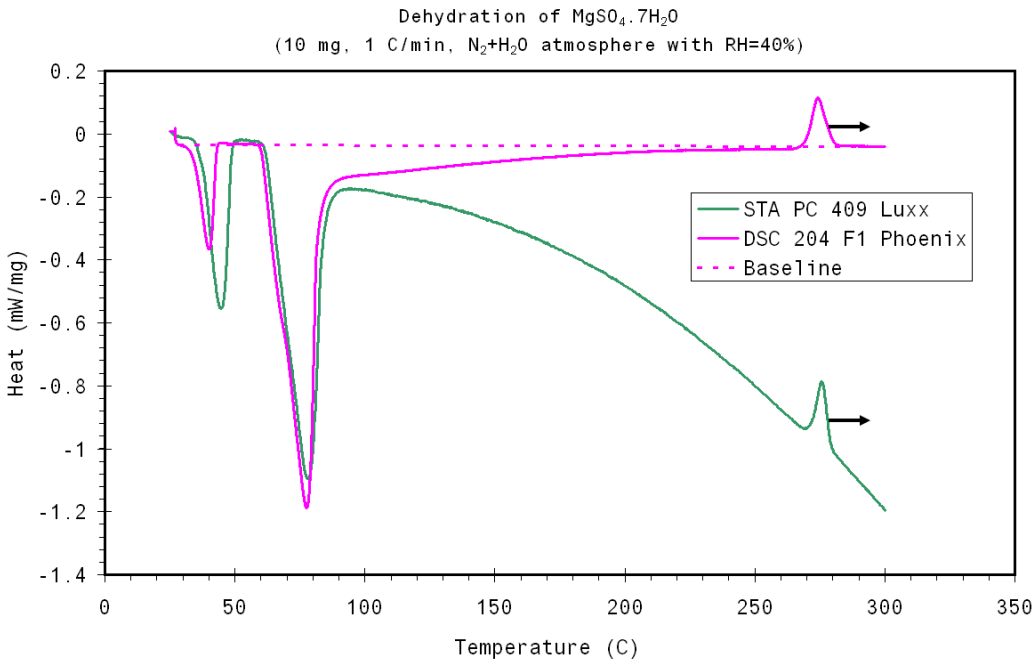


Figure 3: Experimental DSC curves as function of temperature for dehydration of $MgSO_4.7H_2O$ (particle size = 38-106 μm).

The DSC curves obtained using the Netzsch STA PC 409 Luxx apparatus shows a decreasing baseline (green line in Figure 3) when the sample (Merck) was subjected to a $N_2$+$H_2O$ atmosphere. The drifting of the baseline can be an indication of problems with the experimental setup such as instrument malfunction or displacement of crucible. A separate experiment was performed using another DSC machine (Netzsch DSC 204 F1 Phoenix) using $MgSO_4.7H_2O$ from VWR under the same experimental conditions (sample mass, $N_2$+$H_2O$, atmosphere and heating rate). The result of this experiment is shown as the purple line in Figure 3. The DSC curve obtained from this experiment shows a constant baseline. Experts from Netzsch Application Laboratory indicate that usage of a different carrier system compared to the calibration situation could be a reason for this non-constant DSC baseline.
Apart from the first peak, which will be discussed later in this section, the shape and position of the other two peaks corresponds quite well: the difference between the areas under the third peak of the two DSC curves is less than 10%. Since a constant baseline offers more accurate determination of the area under the curves, we will use the DSC curve from the Netzsch DSC 204 F1 Phoenix for determination of the dehydration enthalpy.

Figure 4 shows a combined TG-DSC curve for dehydration of $MgSO_4.7H_2O$:

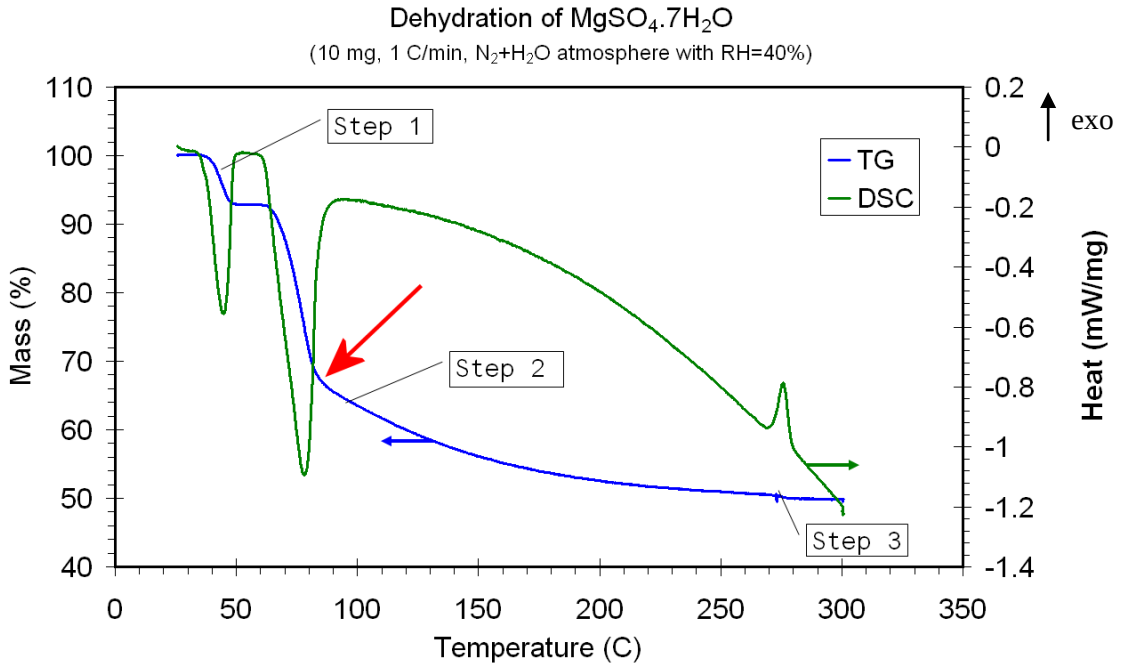


Figure 4: Experimental TG-DSC curve as function of temperature for dehydration of $MgSO_4.7H_2O$ (VWR, particle size = 38-106 μm). The red arrow indicates the inflection point of the change in shape of TG curve at second dehydration step (see text for details)

The TG curve for dehydration of $MgSO_4.7H_2O$ shows that three different steps can be identified: a mass loss between 25°C and ~55°C, a gradual decrease in the mass between 60°C - 265°C and a small decrease at 275°C. Figure 4 also shows that each decrease in TG signal is accompanied with a peak in DSC signal, therefore each step identified in TG curve can be associated with a dehydration reaction. From the TG curve the mass change per step can be calculated and used to identify the amount of expelled water during each dehydration reaction. Table 1 shows the mass change per step as shown in Figure 4:

| Step | Mass loss (%) | Water molecules |
|---|---|---|
| 1 | 6.9±0.2 | 0.9±0.03 |
| 2 | 42.2±0.3 | 5.9±0.04 |
| 3 | 0.5±0.1 | 0.1±0.02 |
| Total | 49.9±0.2 | 6.8±0.03 |

Table 1: Experimental mass changes and expelled water molecules per dehydration step (95% confidence limit, 8 measurements). A mass loss of 7.31% corresponds to the loss of one water molecule.

A total mass loss of 49.9±0.2% was found which is close to the theoretical value of 51.2 % corresponding to 7 water molecules. The first dehydration reaction involves the loss of almost one water molecule and corresponds to the following well-known dehydration reaction:

$$MgSO_4.7H_2O(s) \Rightarrow MgSO_4.6H_2O(s) + H_2O(g) \qquad (R.2)$$

From the shape of the TG curve it can be seen that the second dehydration step at least consists of two dehydration steps: a steep decrease in TG signal is followed by a more gradual decrease in TG signal (see the inflection point indicated by a red arrow in Figure 4). Unfortunately, the gradual decrease in TG signal makes it impossible to clearly identify intermediates formed dur-

ing the dehydration of $MgSO_4.6H_2O$. Based on the mass decrease, the following reaction can be identified:

$$MgSO_4.6H_2O(s) \Rightarrow MgSO_4.0{,}1H_2O(s) + 5{,}9H_2O(g) \quad \text{(R.3)}$$

The third step involves a very small mass decrease at temperatures near 275 °C. This mass decrease was consistently observed during the experiments and is always accompanied by a change in DSC signal, which indicates the following dehydration reaction:

$$MgSO_4.0{,}1H_2O(s) \Rightarrow MgSO_4(s) + 0{,}1H_2O(g) \quad \text{(R.4)}$$

The existence of $MgSO_4.0{,}1H_2O$ seems doubtful and it is most likely that this phase is a mixture of $MgSO_4.H_2O$ and $MgSO_4$. The shape of the TG curve suggests that this last transition is a single step reaction.
Since water vapor influences the DSC signal in Figure 4, it was decided to determine the reaction enthalpy for each dehydration step using the DSC curve measured by Netzsch DSC 204 F1 Phoenix apparatus shown in Figure 3. However, a difference in area under the first peak was observed between the STA and DSC measurement as shown in Figure 3. It should be noted that the DSC curves determined using the Netzsch DSC 204 F1 Phoenix were obtained two months after the DSC curve determined using the STA . Since $MgSO_4.7H_2O$ can dehydrate according to reaction R.1 under lab conditions (see above), it is very likely that the sample used for STA measurements contains more $MgSO_4.6H_2O$. This would also explain the difference in area under the curve: less $MgSO_4.7H_2O$ is converted via reaction R.2 for the sample measured in the Netzsch DSC 204 F1 Phoenix, resulting in less heat released (= a smaller area under the DSC curve). For this reason, enthalpy and energy storage density for the first peak was taken from the area under the DSC curve from STA apparatus (see also Figure 3), since the composition of this material is less affected by "natural" dehydration.
From the DSC curve shown in Figures 3 and 4 it can be seen that the first two dehydration steps are endothermic processes (indicated by the negative DSC signal), while the last dehydration step is exothermic. Table 2 shows experimental enthalpies of reaction ($\Delta_rH$) and energy densities for the three dehydration steps:

| Reaction | $\Delta_rH$ [kJ/mol]* | $\Delta_rH$ [kJ/mol $H_2O$] | Energy storage density $(GJ/m^3)^B$ |
|---|---|---|---|
| $MgSO_4.7H_2O(s) \rightarrow MgSO_4.6H_2O(s) + H_2O(g)$ | 50.2 ± 2.5 | 50.2 ± 2.5 | $0.3 \pm 2\times10^{-2}$ |
| $MgSO_4.6H_2O(s) \rightarrow MgSO_4.0{,}1H_2O(s) + 5{,}9H_2O(g)$ | 318.9 ± 15.9 | 54.1 ± 2.7 | 2.2 ± 0.1 |
| $MgSO_4.0{,}1H_2O(s) \rightarrow MgSO_4(s) + 0{,}1H_2O(g)$ | -15.1 ± 0.8 | -151.1 ± 8.0 | $-0.1 \pm 1\times10^{-2}$ |

* = the enthalpies of reaction are related to one mole of $MgSO_4.7H_2O$. Here an estimated error of 5% was assumed for the determination of the reaction enthalpy.

Table 2: Experimental enthalpies and energy storage densities of the dehydration reactions of magnesium sulfate hydrates.

The lower hydrates are expected to stronger bound the water molecules than the higher hydrates, which is reflected in the higher absolute reaction enthalpy per mole water for the third dehydration step compared to the other two dehydration steps [17].
The experimental values for energy storage density in Table 2 show that the second dehydration step is most interesting for thermal storage, since it corresponds to the largest experimental storage density. In fact, the experimental energy density for the second dehydration reaction is al-

[B] The energy density $\rho_E$ can be calculated by multiplying the reaction enthalpy $\Delta_rH$ [J/mol] with density $\rho$ [g/m3] and dividing it through the molar mass M (g/mol): $\rho_E = \frac{\Delta_r H \cdot \rho}{M \cdot 10^9}\left[\frac{GJ}{m^3}\right]$

most 10 times more energy compared to the value for water in the temperature range of 25-85°C (=0.25 GJ/$m^3$)
Next, the experimental enthalpies of reaction are compared with calculated ones. To do so, we determine the value of $\Delta_r H$ using known standard enthalpies of formation $(\Delta_f H^0)^C$ [16]. Wagman et al [17] presents values of $\Delta_f H^0$ for magnesium sulfate hydrates such as $MgSO_4.7H_2O$, $MgSO_4.6H_2O$ and $MgSO_4$. However, the $\Delta_f H^0$ for $MgSO_4.0{,}1H_2O$ is not known and was determined by fitting enthalpies of formation for hydrates of magnesium sulfate from Wagman et al [17] as function of the amount of hydrated water molecules, as shown in Figure 5 (see also Appendix C):

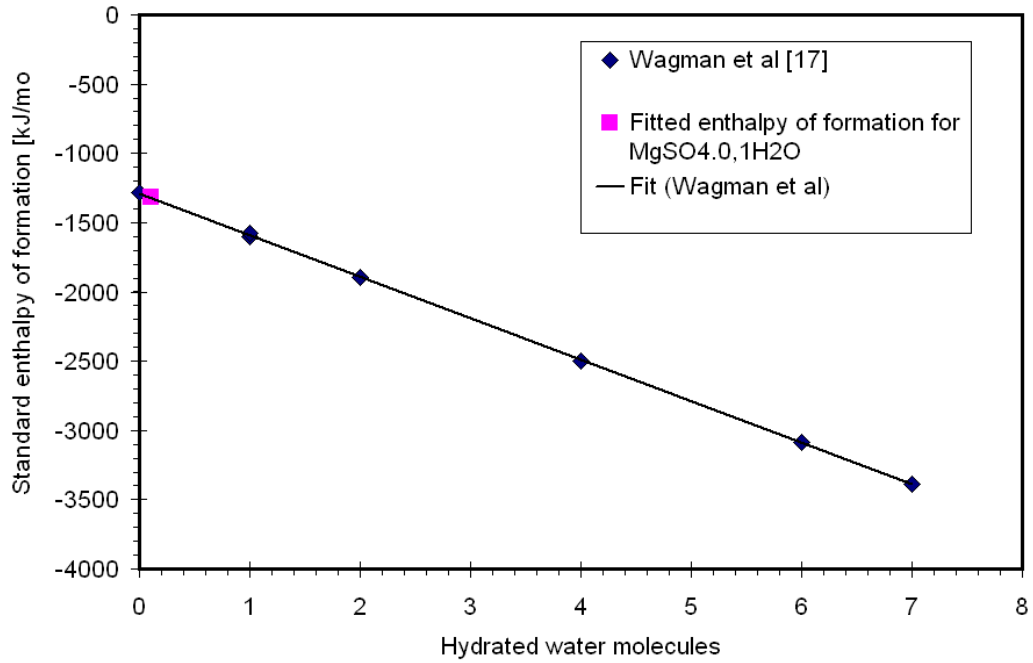


Figure 5: Standard enthalpies of formation for hydrates of magnesium sulfate as function of the number of hydrated water molecules (0=$MgSO_4$, 7=$MgSO_4.7H_2O$) [17]

From the fit a theoretical enthalpy of formation for $MgSO_4.0{,}1H_2O$ of -1319.6 kJ/mol was found. Table 3 shows the experimental and calculated enthalpies of formation for the three dehydration steps:

| Reaction | $\Delta_r H$ [kJ/mol $H_2O$] This study (average value) | $\Delta_r H$ [kJ/mol $H_2O$] Wagman et al [17] | Diff [%] |
|---|---|---|---|
| $MgSO_4.7H_2O(s) \rightarrow MgSO_4.6H_2O(s) + H_2O(g)$ | 50.2 | 59.9 | 19.3 |
| $MgSO_4.6H_2O(s) \rightarrow MgSO_4.0{,}1H_2O(s) + 5{,}9H_2O(g)$ | 54.1 | 57.7 | 6.7 |
| $MgSO_4.0{,}1H_2O(s) \rightarrow MgSO_4(s) + 0{,}1H_2O(g)$ | -151.1 | 60.8 | 140.2 |

Table 3: Comparison between enthalpies of reaction in this study with literature values.

The enthalpy of reaction for the first dehydration reaction is 19.3% lower than the value reported in literature [10, 17]. As mentioned earlier, the reaction enthalpy for the first reaction was determined DSC experiments using the STA at ECN (see also Figure 3). These DSC experiments

[C] The enthalpy of reaction is defined as the difference between the sum of the products and the sum of the enthalpies of reactants: $\Delta_r H = \sum n\Delta_f H_s^0(products) - \sum m\Delta_f H^0(reactants)$, where m and n are stoichiometric coefficients for products and reactants, respectively.

suffers from non-constant baseline, which results in an uncertainty in the determination of the reaction enthalpy (and energy density) since the position of the baseline has to be guessed.
The value of $\Delta_r H$ for the second dehydration reaction shows a good correspondence with the value found in the literature. This gives confidence in the high experimental energy density found for this reaction (see also Table 2).
The experimental value $\Delta_r H$ for the last dehydration reaction shows an exothermic process, which seems odd since the removal of water appears to be endothermic (see also the first and second dehydration steps). In fact, the calculated value of $\Delta_r H$ [17] shows a positive value, which indicates an endothermic process. The observation of a negative $\Delta_r H$ for the final dehydration step in magnesium sulfate-water system is not unique: Ruiz et al [3] also observed an exothermic final dehydration step and found a value of $\Delta_r H$=-13 kJ/mol, which is close to the value found in this study (see also Table 2). According to Ruiz et al [3] the final transition includes an exothermic reaction due to recrystallization of an amorphous precursor, which results in an overall negative enthalpy of reaction.

#### 2.1.2.2 X-ray powder diffraction: dehydration of $MgSO_4.7H_2O$

The suggestion made by Ruiz et al [4] was further investigated by performing X-ray diffraction experiments, where X-ray diffraction patterns were determined during the dehydration of a sample by heating it from 25 °C to 300°C at 1°C/min in gas mixture of nitrogen saturated with water vapor ($P_{H2O}$=2.7 kPa). Figure 6 shows experimental X-ray diffraction patterns for dehydration of $MgSO_4.7H_2O$:

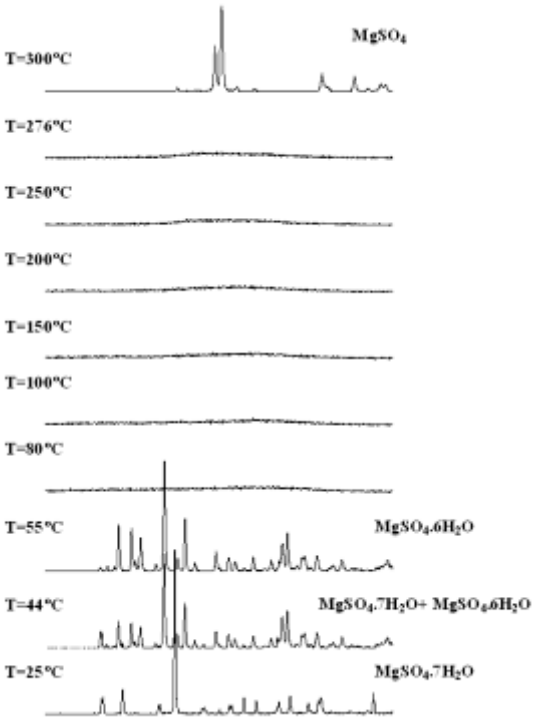


Figure 6: Experimental X-ray diffraction pattern for dehydration of $MgSO_4.7H_2O$. In this case the material supplied by Merck was used (38-106μm).

The above Figure shows X-ray diffraction patterns determined at specific temperatures. Apart from a difference in peak intensity (see above), the experimental results for material supplied by Merck and VWR were identical and for this reason only the experimental X-ray diffraction pattern for Merck is shown. Prior to experiments the sample was subjected for one night to a nitrogen-water atmosphere ($P_{H2O}$=2.7 kPa) until pure $MgSO_4.7H_2O$ was formed, which was confirmed by X-ray diffraction patterns (see T=25°C in Figure 6). When the temperature of the

sample is increase, the X-ray diffraction patterns show that $MgSO_4.7H_2O$ is completely converted to $MgSO_4.6H_2O$ at T=55°C. This observation is in agreement with the results obtained by TG-DSC experiments (see above). The X-ray diffraction patterns for temperatures between T=80°C and 276°C show that at these temperature an amorphous phase is formed. Finally, crystalline $MgSO_4$ is formed at T=300°C, which confirms the findings from TG-DSC curves that the materials is completely dehydrated at this temperature.
A close examination of the X-ray diffraction patterns in the temperature range of 80°C to 276°C reveals a small and broad peak which shifts at higher temperatures. Figure 7 shows this peak together with theoretical X-ray diffraction patterns:

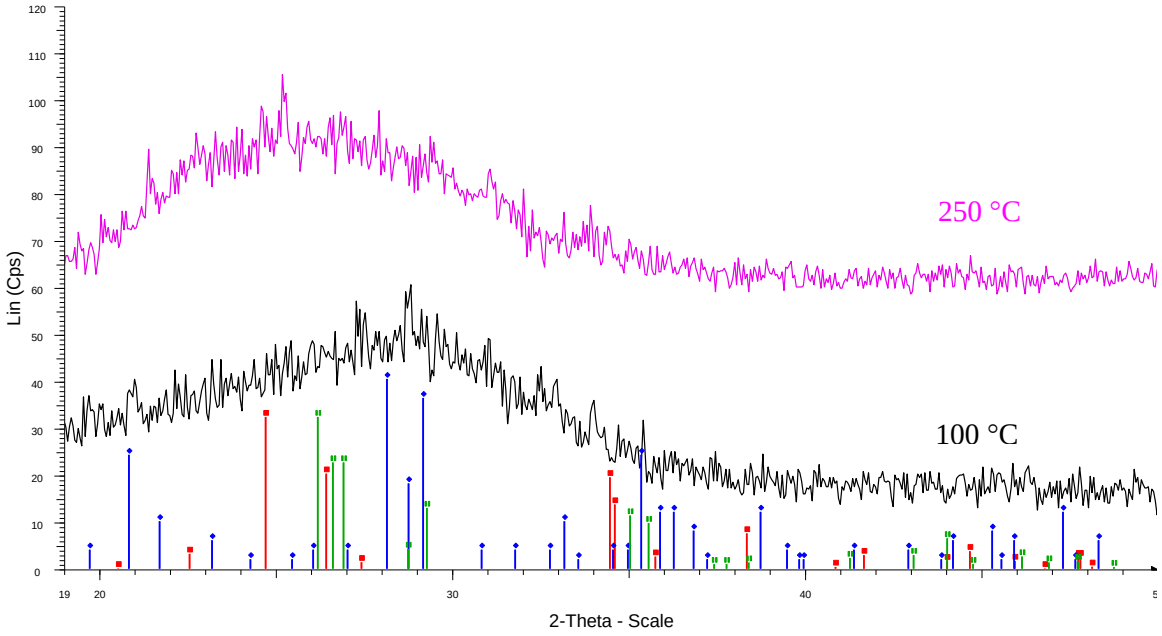


Figure 7: Experimental X-ray diffraction pattern for dehydration of $MgSO_4.7H_2O$ at T=100°C and 250°C. The blue bars denote $MgSO_4.3H_2O$, red bars denote $MgSO_4$ and green bar denote $MgSO_4.H_2O$ theoretical X-ray diffraction patterns

The experimental X-ray diffraction pattern at T=100°C shows some correspondence with the theoretical X-ray diffraction pattern of $MgSO_4.3H_2O$. This observation is in agreement with the results from Emons [5], who found that $MgSO_4.3H_2O$ was formed at 105°C during the dehydration of $MgSO_4.7H_2O$. At T=250°C, the peak of the X-ray diffraction pattern is shifted. According to Emons [5] only $MgSO_4.H_2O$ exists at this temperature, but the theoretical X-ray diffraction pattern shown in Figure 7 shows more correspondence to the theoretical patterns of both $MgSO_4.H_2O$ and $MgSO_4$. This results supports the suggestion that at this temperature a mixture of $MgSO_4.H_2O$ and $MgSO_4$ is formed which was identified as $MgSO_4.0{,}1H_2O$ in the TG-DSC experiments (see above). Summarizing the above, it appears the following intermediates are formed during the second dehydration step:

$$MgSO_4.6H_2O \xrightarrow{T=100^oC} MgSO_4.3H_2O \xrightarrow{T=250^oC} MgSO_4 + MgSO_4.H_2O \text{ mixture} \qquad (R.5)$$

### 2.1.2.3 Melting of the material during dehydration

Initial experiments performed by Van der Voort [13] revealed that the material melts during dehydration. The temperature at which melting occurs is investigated by means of a combined

TG-DSC measurement: the melting process results in a peak in DSC curve without an accompanied change in mass. Based on TG-DSC measurements it was observed that melting only occurs during the first dehydration step. Figure 8 shows differential mass (dTG/dt) and DSC curve for the first dehydration step as function of the temperature:

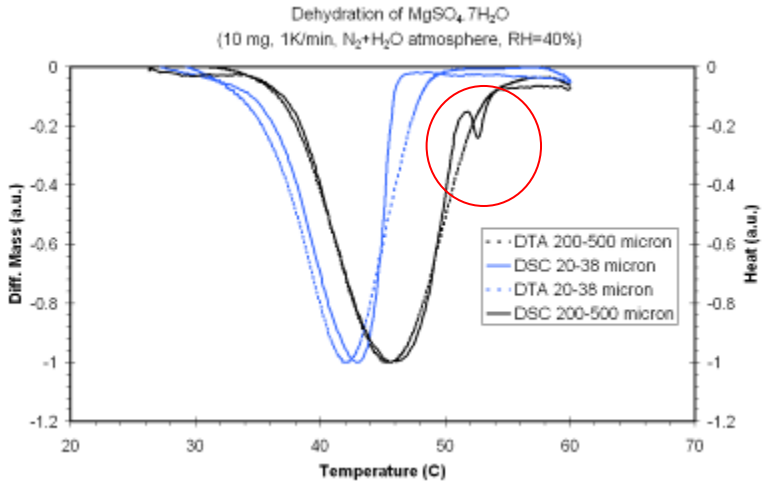


Figure 8: Differential mass and heat as function of temperature for 200-500 and 20-38 μm particles. The red circle indicates the peak associated with melting.

As shown in the above Figure, melting occurs near 52°C, which is in good agreement with the melting temperature of 52.5°C determined by Van der Voort [13] and 50°C determined by Emons et al [5]. If dehydration is slow compared to the heating rate, $MgSO_4.7H_2O$ may still be present at this temperature range and will start to melt incongruently [5]. Further investigation showed that melting doesn't occurs when low heating rates (≤1 °C/min), small particles (<200μm) and/or small sample sizes (<5 mg) are being used. In these cases, dehydration proceeds fast enough compared to the heating rate and $MgSO_4.7H_2O$ will not be present at 52°C.

### 2.1.2.4 Thermal analysis: kinetics analysis of $MgSO_4.6H_2O$ dehydration

#### 2.1.2.4.1 Theory of kinetic analysis

In the previous section the three dehydration steps in the magnesium-water system were identified. If we can determine how different experimental conditions (temperature, water vapor pressure and so on) can influence the reaction rate, we can make a mathematical model to predict effect of each parameter in advance. The information from mathematical model will also help us to find and design the TCM reactor for seasonal heat storage.
In solid-state reactions the reaction rate is generally expressed in terms of fraction of sample reacted [18], which is defined as:

$$\alpha = \frac{m_i - m(t)}{\Delta m} \qquad (1)$$

Where $m_i$ and m (t) are the initial mass and the mass at time t [mg], and Δm is the total mass difference between initial and final mass [mg].

The rate of thermal decomposition of a solid is generally expressed as:

$$\frac{d\alpha}{dt} = k(T) f(\alpha) \qquad (2)$$

Where $\frac{d\alpha}{dt}$ is the reaction rate [$s^{-1}$], k (T) is the temperature dependent reaction rate constant [$s^{-1}$] and f ($\alpha$) is the reaction type. The Arrhenius equation is often used to describe the temperature dependency of the reaction rate constant:

$$k(T) = A\exp\left(\frac{-E}{RT}\right) \tag{3}$$

Where A is the pre-exponential factor [$s^{-1}$], E is the activation energy [kJ/mol] and R is the universal gas constant [kJ/mol.K].Substitution of equation (3) in (2) results in the following expression:

$$\frac{d\alpha}{dt} = A\exp\left(\frac{-E}{RT}\right) f(\alpha) \tag{4}$$

Under isothermal conditions, the sample is heated with a constant heating rate ($\beta = dT/dt$ [°C/s]). In this case, equation (4) can be rewritten as follows:

$$\frac{d\alpha}{dT} = \frac{A}{\beta}\exp\left(\frac{-E}{RT}\right) f(\alpha) \tag{5}$$

The integral form of equation (2 or 5) can be written as:

$$g(\alpha) = \int \frac{d\alpha}{f(\alpha)} = \int k(T)dt = \int \frac{A}{\beta}\exp\left(\frac{-E}{RT}\right)dT \tag{6}$$

Examples of the integral form of the reaction type are listed in Table 4:

| **g(α)** | **Reaction type** |
|---|---|
| -ln(1-α) | First order reaction |
| 1/(1-α) | Second order reaction |
| $\frac{(1-\alpha)^{1-n}}{n-1}$ | $N^{th}$ order reaction (N>1) |
| $\alpha^2$ | One dimensional diffusion |
| $[-\ln(1-\alpha)]^{2/3}$ | one-dimensional nucleation (Avrami/Erofeev, n=1.5) |
| $[-\ln(1-\alpha)]^{1/2}$ | Two dimensional nucleation (Avrami/Erofeev, n=2) |
| $[-\ln(1-\alpha)]^{1/3}$ | Three dimensional nucleation (Avrami/Erofeev, n=3) |
| $[-\ln(1-\alpha)]^{1/n}$ | n dimensional nucleation (Avrami/Erofeev, n=1.5, 2, 3 or 4) |

Table 4: examples of reaction type and corresponding reaction equation [18-21]

Temperature, heating rate and sample reacted are variables that can be retrieved from experiments, but the other parameters for describing the kinetics (pre-exponential factor, activation energy and reaction type) are unknown. To retrieve information on these kinetic parameters, so-called model-fitting is used, which solves equation (6) by fitting experimental data to different reaction types. For each reaction type, the fit will also give fitted values for the activation energy and pre-exponential factor.
The kinetic software from Netzsch (version 2006.08) [22] was used for the kinetic analyses of the dehydration measurements. This software package includes 16 reaction types to fit the experimental data.

#### 2.1.2.4.2 Experimental details

Experimental TG curves using the STA apparatus served as input for kinetic software. Table 5 gives an overview of the experimental conditions:

| | |
|---|---|
| Heating rates | 0.5, 1, 5 and 10 °C/min |
| Temperature range | 25°C…300°C |
| Mass | 10 mg |
| Atmosphere | nitrogen |
| Starting material | $MgSO_4.6H_2O$ |

Table 5: Experimental conditions for TG measurements

The kinetic software is able to simultaneous analyze multiple TG curves. It was decided to perform TG measurements run at four heating rates instead of a single heating rate: more and accurate information is obtained compared to a single run, which improves the selection of the reaction type [23]
Because we were not sure about the partial water vapor pressure used during the STA measurement, it was decided to perform the measurements in a dry nitrogen atmosphere. After the experiments were performed it was discovered that the starting material was completely converted to $MgSO_4.6H_2O$. This means that the kinetic analysis of the first dehydration step was not possible. The last dehydration step could also not be evaluation since the mass difference was too small.
Thus, only the second dehydration step could be analyzed, which is not bad since this step is the most interesting for seasonal heat storage (see previous section).

#### 2.1.2.4.3 Kinetic analysis of second dehydration step.

From the TG-DSC curves discussed in the previous section, it was determined that the second dehydration step involves several dehydration steps. The best way to fit the kinetic parameters of this complex reaction is to use a non-linear regression [23], which is an iterative process. This process requires a set of initial values (or initial guesses) in order to be able to fit the experimental data. These initial values can be acquired by using a model-free estimation of the activation energy as described by Ozawa, Flynn and Wall (OFW) [23]. The result of this model-free estimation is presented in Figure 9:

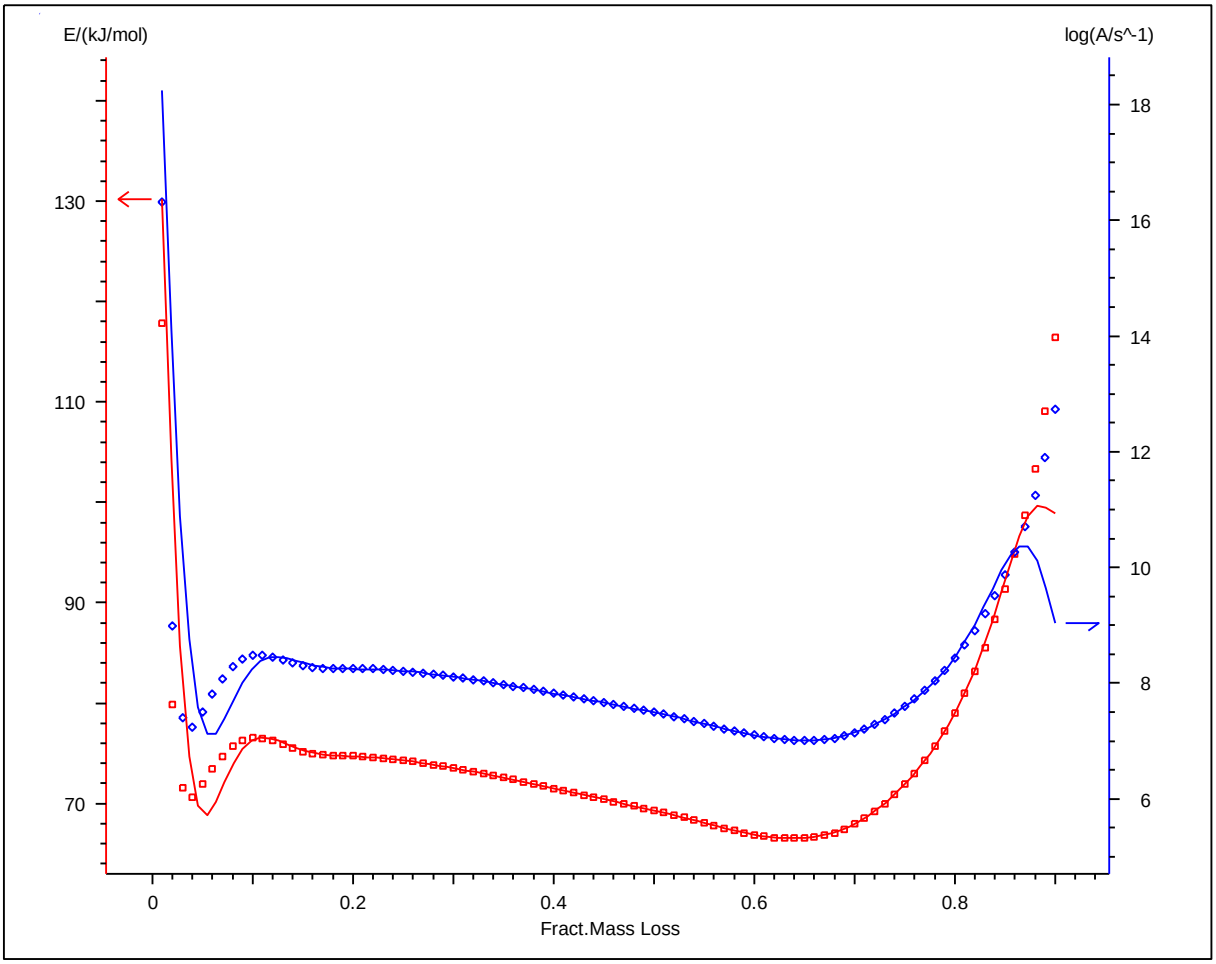


Figure 9: Activation energy and pre-exponential factor as function of the fraction mass loss (0=no mass loss, 1 = total mass loss). The dots denote experimental values; the lines denote fits based on model-free estimation [22, 23]

The above Figure shows that the activation energy changes as function of the fraction mass losses. Three regions can be identified as shown in Table 6:

| Fraction mass losses | Activation energy (kJ/mol) |
|---|---|
| 0.0-0.05 | 70-130 |
| 0.05-0.6 | 70-80 |
| 0.6-1.0 | 70-100 |

Table 6: Overview of regions with different behavior of activation energy as function of fractional mass loss

Each region shows a different behavior of the activation energy as function of the fraction mass loss; the first and third region show a rapid change in activation energy and the second show a more constant value for the activation energy. This behavior of the activation energy is an indication that the reaction contains at least three steps. The values of the activation energy and pre-exponential factor for each region were determined from Figure 9 and used as initial value for the non-linear regression fit. The TG curves were fitted to 18 mechanism functions[D]. The best result is shown in Figure 10:

[D] A mechanism function is consisting of one or more reaction types, for example: a first order reaction followed by an $n^{th}$ order reaction.

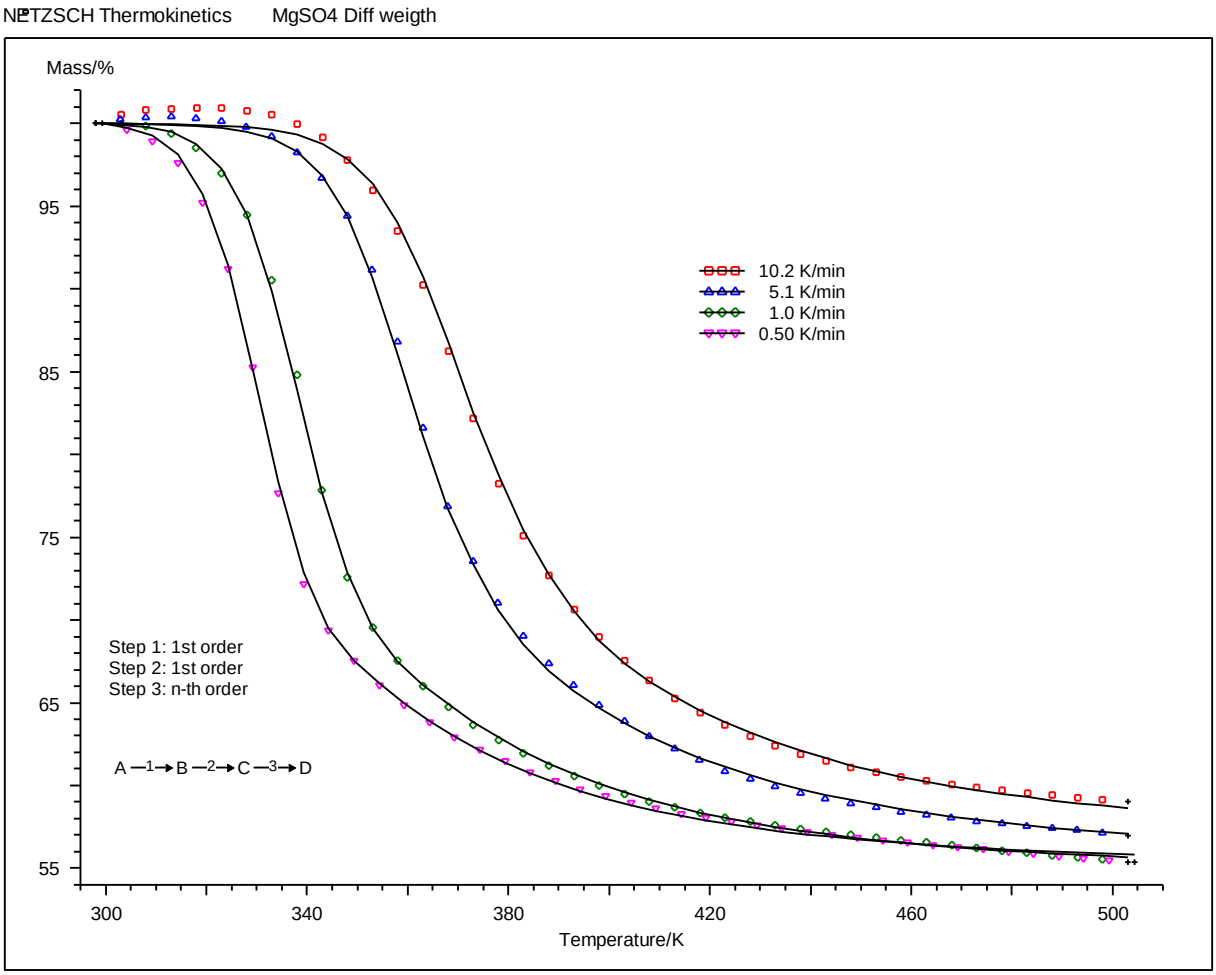


Figure 10: Kinetic analysis of the TG curves as function of temperature for the dehydration of $MgSO_4.6H_2O$. Dots denote measured values, lines denote fit.

The above fit was achieved when a three-step consecutive reaction was fitted where the first two reaction steps were 1st order and the last reaction step was nth order. As can be seen in Figure 10, the fit describes the dehydration of $MgSO_4.6H_2O$ quite well. It is therefore recommended to use the kinetic parameters shown in Table 7 for describing the dehydration of $MgSO_4.6H_2O$ in a nitrogen atmosphere:

| Step | Corresponding transition | Reaction order | $E_a$ (kJ/mol) | Log A ($s^{-1}$) |
|---|---|---|---|---|
| 1 | $MgSO_4.6H_2O \rightarrow MgSO_4.5{,}7H_2O$ | 1 | 89.2±4.4 | 11.4±0.7 |
| 2 | $MgSO_4.5{,}7H_2O \rightarrow MgSO_4.2{,}3H_2O$ | 1 | 59.7±7.7 | 6.5±1.0 |
| 3 | $MgSO_4.2{,}3H_2O \rightarrow MgSO_4.0{,}4H_2O$ | 4 | 74.0±6.0 | 7.6±0.8 |

Table 7: Optimized kinetic parameters for dehydration of $MgSO_4.6H_2O$. The correlation coefficient of the fit was 0.999803

### 2.1.3 Water uptake of dehydrated material

After dehydration, the anhydrous $MgSO_4$ was allowed to hydrate at 25°C for 20 hours in a gas mixture of water and nitrogen. As mentioned earlier, the relative humidity during the experiments performed at ECN were assumed to be 40% or $P_{H2O}$ = 1.3 kPa (at 25°C). In this section the experiments performed on the STA (TG-DSC), DSC machine and X-ray diffraction apparatus at ECN are discussed.

#### 2.1.3.1 Thermal analyses: water uptake by $MgSO_4$

The dehydration experiments described in the previous section showed that $MgSO_4$ was formed after $MgSO_4.7H_2O$ was heated up to 300°C. After $MgSO_4$ was cooled down to 25°C with -5 °C/min, the material was allowed to hydrate for 20 hours in the gas mixture of water and nitrogen (assuming RH=40% or $P_{H2O}$ = 1.3 kPa above the sample). Figure 11 shows typical TG-DSC dehydration curves for material from both VWR and Merck:

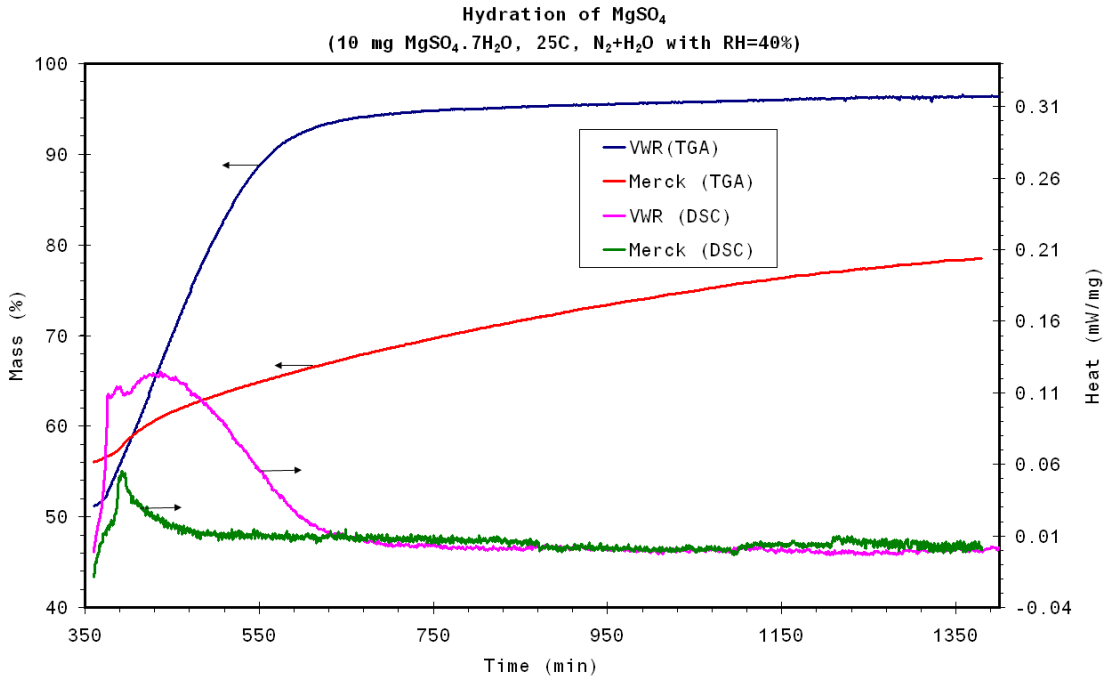


Figure 11: Experimental TG-DSC curves for hydration of $MgSO_4$ at 25°C and RH=40% (see text for details)

In general, the experimental results indicate that the dehydrated material is able to take up water while releasing heat (positive peaks in DSC curve in the above Figure). However, the extent of the water uptake is dependent on whether the material is from Merck or VWR. The material from Merck starts at a higher mass percentage then the material from VWR. This difference can be traced back to the difference in composition of the starting material prior to the dehydration reaction (see also section 2.1.1)
The shape of the TG curve for the material from Merck shows a gradual and slow uptake of water. The total mass increase after 20 hours was ~19.3±2.1% (95% confidence limit, 4 measurements) which corresponds to the following reaction:

$$MgSO_4(s) + 2{,}6H_2O\ (g) \rightarrow MgSO_4.2{,}6H_2O(s) \qquad (R.6)$$

On the contrary, the material from VWR is characterized by a much faster hydration: in 5 hours the total mass increase was 44.5±0.9% (95% confidence limit, 10 measurements) which corresponds to:

$$MgSO_4(s) + 6H_2O\ (g) \rightarrow MgSO_4.6H_2O(s) \qquad (R.6)$$

The shape of the TG curve suggests that the water uptake by the material from VWR proceeds as a single step reaction.
For thermo chemical heat storage applications it is necessary that the heat stored during dehydration is released during hydration. However, the DSC hydration curve for Merck's material shows almost no heat release, whereas the DSC hydration curve for material from VWR clearly shows an exothermic (positive) peak. The difference in heat release is a consequence of the difference in hydration speed: if it is slow, the heat release is also slow. In case of material from Merck, the heat release (hydration) is so slow that it almost cannot be detected by means of DSC. For this reason, the enthalpy of hydration was only determined for the material from VWR. The enthalpy of hydration is shown in Table 8 and compared to enthalpy of dehydration (see also previous section):

| | Dehydration* | Hydration |
|---|---|---|
| Overall reaction | $MgSO_4.6H_2O(s) \rightarrow MgSO_4(s) + 6H_2O(g)$ | $MgSO_4(s) + 6H_2O\ (g) \rightarrow MgSO_4.6H_2O(s)$ |
| Total enthalpy (kJ/mol) | 303.8 ± 15.2 | 268.4 ± 13.4 |
| Total energy storage density ($GJ/m^3$) | 2.1 ± 0.1 | 1.8 ± 0.1 |

* = values were obtained by adding enthalpies and energy storage densities for the second and third dehydration steps 2 and 3 (see also Table 2)

Table 8: overview of hydration and dehydration enthalpies and energy storage densities

The values for the enthalpy of hydration and dehydration are in close agreement (approximately 14%), which indicates that the amount of stored heat can be retrieved after one dehydration-hydration cycle.
From the above description of difference in hydration between two powder materials, the material supplied by VWR seems more interesting as thermochemical material since hydration is fast and heat release is clearly noticeable. For this reason we will only discuss the hydration results obtained by using VWRs material.

#### 2.1.3.2 X-ray diffraction

The water uptake of the dehydrated material (from VWR) was also investigated using X-ray diffraction. First, the powder material was dehydrated under nitrogen atmosphere by heating it up from 25°C to 300°C with 1°C/min. After the formation of the anhydrous material at 300°C, which was confirmed by X-ray diffraction pattern (see Figure 12), the material was cooled down to 25°C overnight. At this temperature the material was subjected to a water nitrogen atmosphere ($P_{H2O}$=2.7 kPa). The results are shown in Figure 12:

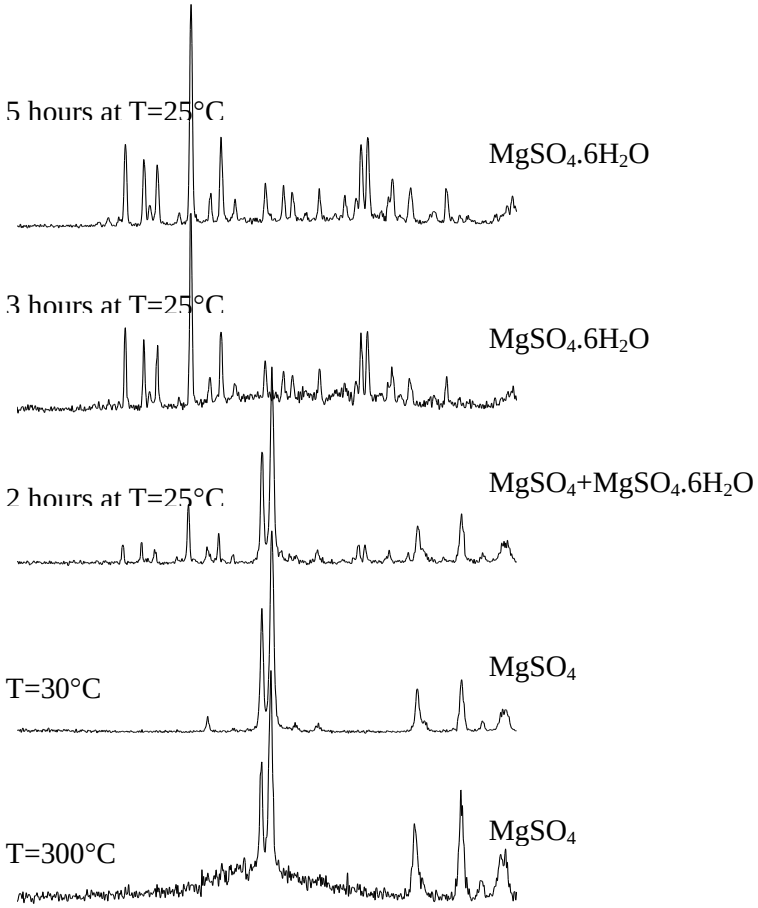


Figure 12: Experimental X-ray diffraction patterns: at T=300°C and 30°C, the material was subjected to $N_2$ atmosphere, while at 25°C a $N_2$+$H_2O$ atmosphere ($P_{H2O}$=2.7 kPa) was applied.

The dehydrated material takes up water and forms $MgSO_4.6H_2O$ without the formation of intermediates, which was also observed in the TG-DSC experiments. The material is converted to $MgSO_4.6H_2O$ in 3 hours, which is shorter than the 5 hours found in the TG-DSC experiments. The differences in water vapor pressure, 2.7 kPa during X-ray diffraction compared to an estimated 1.3 kPa applied during TG-DSC experiments, is most likely the reason for this difference.

### 2.1.3.3 Kinetics of $MgSO_4$ hydration

The hydration experiments using material supplied by VWR were all performed at T=25°C, which means that only the reaction rate constant k (T) at T= 25°C can be determined. It should be noted that in case of hydration, the dehydrated fraction starts from $\alpha$=1 (see equation (1), fully dehydrated or $MgSO_4$) to $\alpha$ =0 (fully hydrated or $MgSO_4.7H_2O$). Since the final product in the hydration of $MgSO_4$ (supplied by VWR) is $MgSO_4.6H_2O$, it means that the value of $\alpha$ ranges from 1 to 0.14, as shown in Figure 13

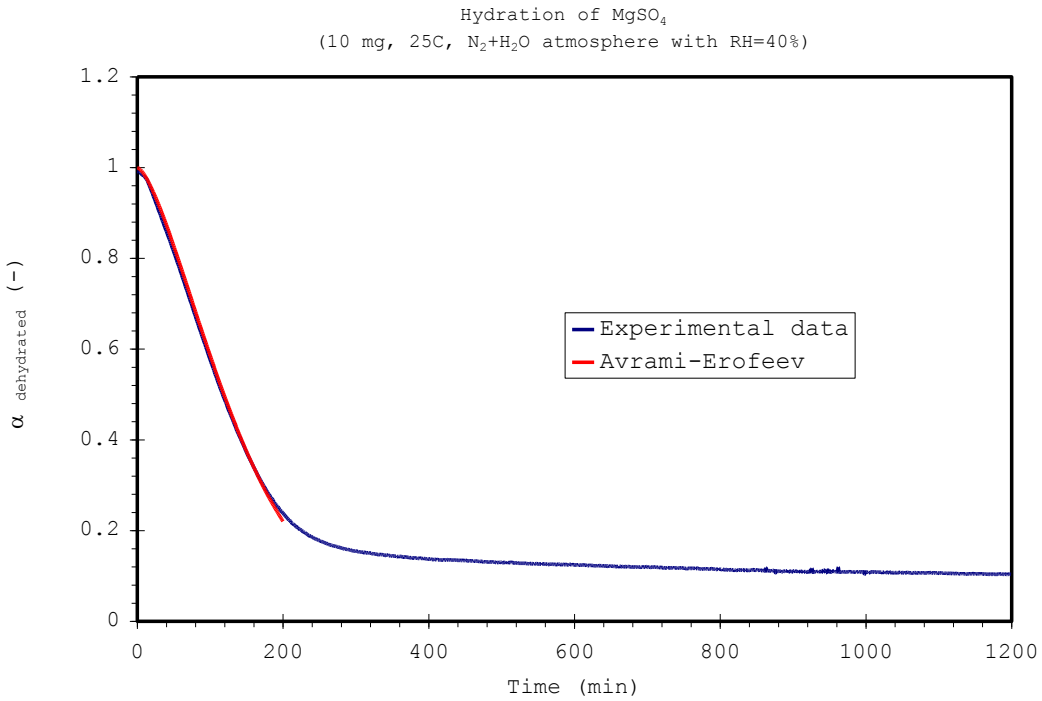


Figure 13: Dehydrated fraction as function of time. Blue line denotes experiment, purple line denotes fit based on Avrami-Erofeev model (particle size = 38-106 μm)

The above Figure shows that the dehydration fraction decreases linear in time for α=1-0.2. As a first rough estimation of kinetic parameters, several empiric equations were fitted to this linear part using MS Excel. It turns out that the Avrami-Erofeev model[E] (see also Table 4) for n=1.5 [8, 9] was most appropriate for hydration:

$$\alpha_{dehydr}(t) = \exp\left[-\left(k\left(T = 25^{\circ}C\right)\cdot t\right)^{1.5}\right] \qquad (7)$$

Where k (25°C) =0.00658 $min^{-1}$ is the fitted reaction rate constant at 25°C and t is time [min]. Equation (7) showed an excellent fit in the dehydration fraction range of 1-0.2 (see also Figure 13) which corresponds to the following hydration reaction:

$$MgSO_4(s) + 5{,}6H_2O(s) \rightarrow MgSO_4.5{,}6\ H_2O(s) \qquad (R.7)$$

However, it should be noted that although the fit looks good, it is still a fit at single temperature and single partial water vapor pressure: simultaneous fitting of TG-curves acquired at different hydration temperatures and controlled water vapor pressure(s) is highly recommended [23] for more accurate determination of kinetic parameters for hydration of $MgSO_4$ to $MgSO_4.6H_2O$.

[E] The Avrami-Erofeev kinetics is an indication that the reaction rate is determined by the formation and growth of product nuclei.

### 2.1.4 The effect of particle size and layer thickness during the dehydration and hydration processes

In the previous section the reactions involved during dehydration and hydration of the material were discussed. The results indicated that the material could be dehydrated and, subsequently, take up water. In this section the effect of dehydration and hydration on the particle (grain) is discussed based on the SEM experiments.
The results discussed in the previous section are based on using particles of 38-106 μm. Van der Voort [13] discovered that the size of the particle and also the layer thickness influences the dehydration process. To further investigate this, it was decided to perform TG-DSC experiments using different particles ranging from 20-500μm. Additionally, the layer thickness was varied by performing experiments with different sample masses using the same type of crucible during TG-DSC experiments.

#### 2.1.4.1 The effect of dehydration and hydration on grains

To investigate the effect of dehydration on a grain, it was decided to make SEM pictures of grains (38-106 μm) before and after dehydration, and after hydration. The dehydration took place by heating the sample from 25 °C to 150°C with 1°C/min. After cooling down to room temperature (25°C), the material was allowed to take up water under ambient conditions (RH~50-55%). Figure 14 shows the results of these experiments for the material from Merck:

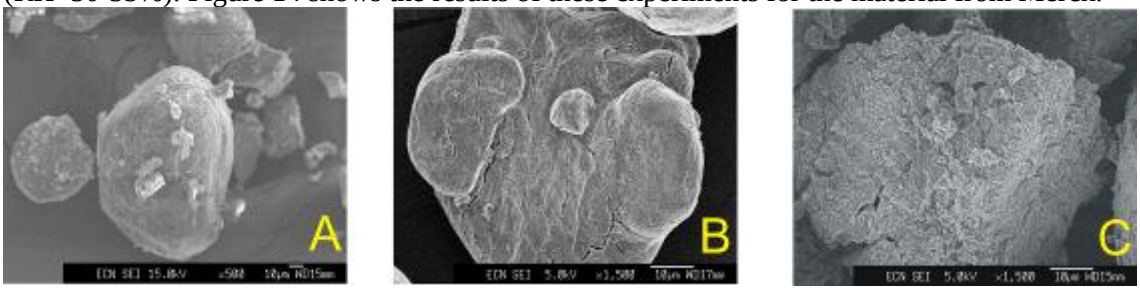


Figure 14: SEM pictures of particles (38-106 μm) for material from Merck: A; before dehydration, B; after dehydration, C: after hydration. The material was dehydrated to 150°C with 1 °C/min and hydrated at ambient conditions

And for the material from VWR are shown in Figure 15:

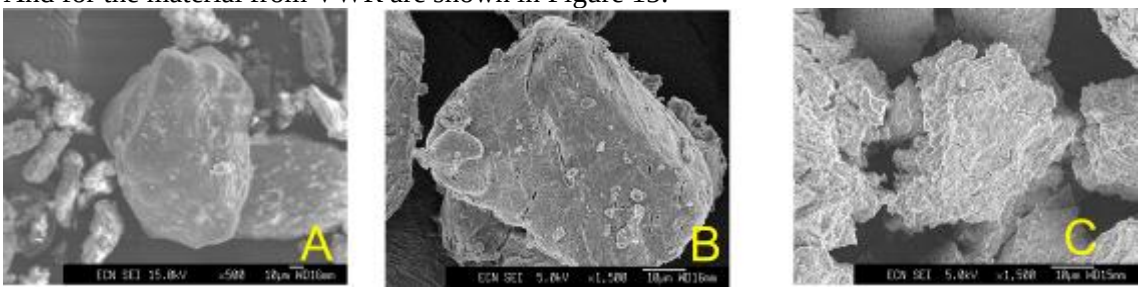


Figure 15: SEM pictures of particles (38-106 μm) for material from VWR: A; before dehydration, B; after dehydration, C: after hydration. The material was dehydrated to 150°C with 1 °C /min and hydrated at ambient conditions.

The same trend can be observed for both Merck and VWR supplied material: before hydration the surface of the grain is smooth, but after dehydration cracks appear due to the release of water vapor and when the materials takes up water the grains appear to be more porous (more cracks appear). The porous structure of the grain seemed unaltered when the material was dehydrated again; even after several cycles the grain did not visually become more or less porous (see also Appendix D). The SEM experiments indicate that there is no noticeable visual differ-

ence between material from Merck and VWR. Additional porosity[F] measurements (see Appendix E) indicate that after dehydration the porosity of both materials is similar:

| | Merck | VWR |
|---|---|---|
| Porosity between particles (vol %) | 12.7 | 14.1 |
| Porosity of particles (vol %) | 54.2 | 54.5 |

Table 9: Values for porosity (vol %) for material from Merck and VWR after dehydration of the material. The same experimental conditions as for the SEM experiments were used.

These SEM pictures and the porosity measurements suggest that there is no difference in porosity between the material from VWR and Merck, which indicates that the difference in water uptake (see also § 3.1.3.1) cannot be explained based on processes occurring on a grain level.
Next, the particle distribution of particles before and after dehydration, and after hydration was investigated. Figure 16 shows the results of these measurements:

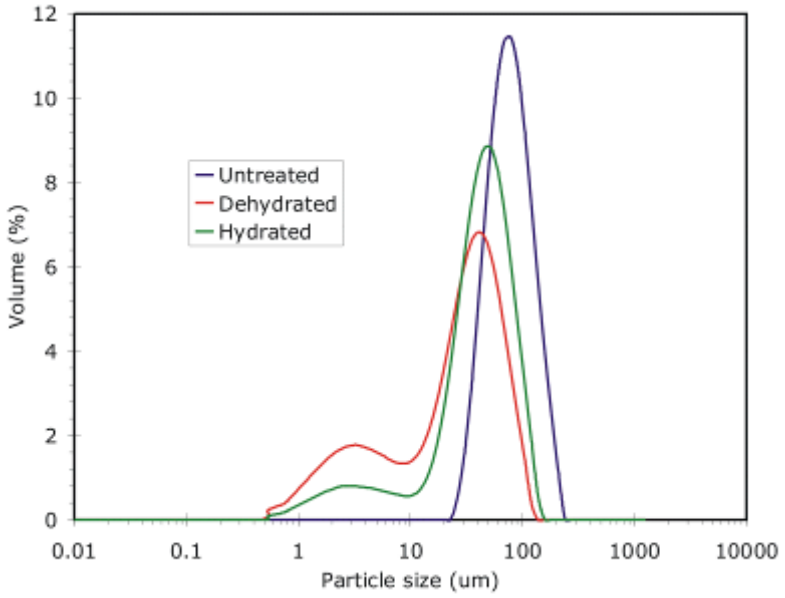


Figure 16: Particle size distribution of $MgSO_4.7H_2O$ (Merck): before (blue line) and after (red line) dehydration, and after hydration (green line). The material was dehydrated to 300°C with 1 °C/min and hydrated under ambient conditions.

The material was sieved to acquire particles of 38-106μm prior to the experiments. The particle distribution before dehydration (blue line in Figure 16) shows a good correspondence between the expected particle distribution based on sieving the material and the actual particle distribution. After dehydrating the material, the particle distribution shifts to smaller particle sizes and in particular particles ranging 1-10μm have formed. It seems that the formation of cracks in the particles (see Figure 14) can be so violent that smaller particles are ejected from the particle. The formation of small particles can be a problem for a future TCM reactor; for example, when a fluidized bed is used the smaller particles could flow out of the reactor before being dehydrated [27]. When the dehydrated material takes up water, the particle sizes distribution slightly shifts to larger particles due to the crystal growth.
The hydration reaction results in a significant variation in molar volume (3 times) between the reactant ($MgSO_4$) and the (final) product, which is assumed to be $MgSO_4.6H_2O$[G]. The particle size distribution changes to smaller particles when the material dehydrates, which is surprising when considering the large variation in molar volume. A possible explanation for this behavior is that the grain size remains constant but the porosity of the grain changes upon hydration and dehydration. However, more research is needed to fully understand this behavior. The particle

[F] The porosity is defined as the volume of the void-space divided by the total or bulk volume of the material
[G] The molar volume ($cm^3$/mol) is calculated by dividing the molar mass through the density of the material. The calculated molar volume for $MgSO_4$ is 0.05 $cm^3$/mol and for $MgSO_4.6H_2O$ is 0.15 $cm^3$/mol.

distribution measurement was only determined for the material from Merck, but it is assumed that the material from VWR shows similar behavior since the SEM pictures.

#### 2.1.4.2 Effect of particle size on hydration and dehydration of the material

To investigate the effect of particle size on dehydration, it was decided to study the dehydration for particle sizes of 20-38µm, 38-106µm, 106-200µm and 200-500µm. The sample weight was held constant to 10 mg. Since the material from VWR appeared to take up more water than the material from Merck, it was decided to use the former to investigate the influence of the particle size and layer thickness. Figure 17 shows TG dehydration curves for different particle sizes:

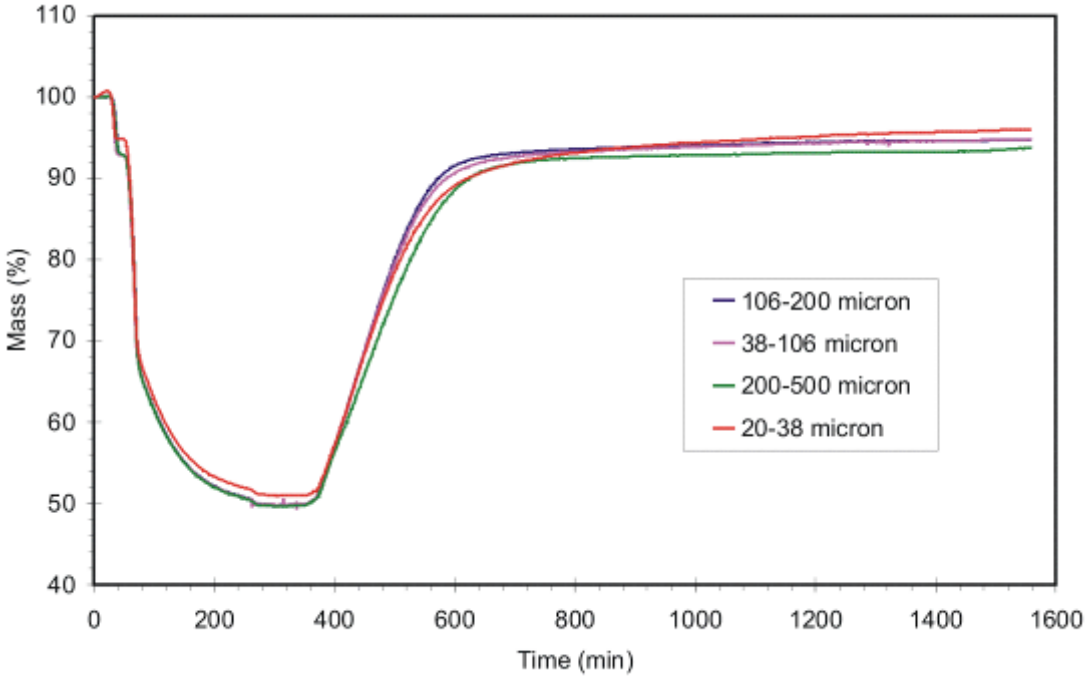


Figure 17: TG curves as function of temperature for four different particle size distributions for material from VWR. The material (10 mg) was dehydrated from 25-300°C (1 °C/min) and hydrated at 25°C under $N_2$+$H_2O$ atmosphere with RH~40%.

The shape of the dehydration (first part till ~400 minutes) and the hydration (between 400-1600 minutes) TG curves is similar to the ones previously discussed (see also Figure 2 and Figure 11). The results in the above Figure clearly indicate the investigated particle sizes don't influence both hydration and dehydration.

#### 2.1.4.3 Effect of layer thickness on dehydration and hydration of the material

Van der Voort [13] indicated that very large layer thickness significantly decelerates the propagation of the dehydration reaction. In addition to this, the low thermal conductivity of salt hydrates will mean that thick layers require more time to dehydrate. Van der Voort [13] performed experiments on two different layer thicknesses and using high (30 K/min) heating rates. The goal of the experiments described here is to study the effect of layer thickness on the dehydration reaction using a smaller heating rate (1 K/min) in order to avoid melting of the material during the first dehydration reaction (see above). The effect of layer thickness was studied by varying the mass, but keeping the particle size (38-106µm) constant. The experiments were performed using crucibles with a volume of 72 $mm^3$. Since the dimensions of the crucible remained constant (same crucible was used), it is possible to change the layer thickness by varying the

mass. Table 10 gives an overview of the masses used during the experiments and their corresponding (calculated) layer thickness.

| Mass (mg) | Layer Thickness (mm) |
|---|---|
| 5 | 0.1 |
| 20 | 0.4 |
| 50 | 1.1 |

Table 10: variation in mass and corresponding layer thickness.

Again, in order to clearly see any differences during hydration and dehydration it was decided to choose the material from VWR as starting material since this material shows a larger water uptake. The results of the TG experiments are shown in Figure 18:

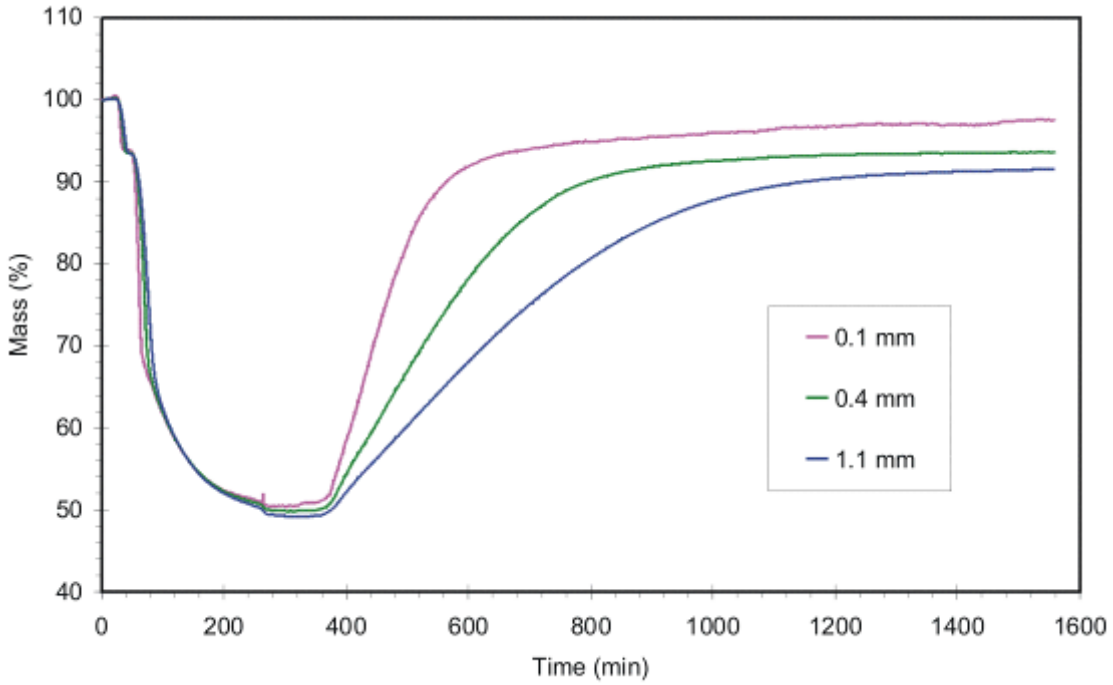


Figure 18: TG curves as function of temperature for three different values for the layer thickness (material from VWR). The material (10 mg) was dehydrated from 25-300°C (1 °C/min) and hydrated at 25°C under $N_2$+$H_2O$ atmosphere with RH~40%.

Hydration, and to a lesser effect the dehydration, is strongly affected by a change in layer thickness: a smaller layer thickness, the reaction is completed in a shorter time, which is in agreement with the findings of Van der Voort [13]. For a future TCM reactor it means that the effect of layer thickness cannot be ignored; although small samples were used, the observed trend indicates that increasing the layer thickness may result in slower water uptake.
Summarizing the above results on the effect of particle size and layer thickness: it can be said that the effect of particle size is limited, but the layer thickness influences the hydration rate. The layer porosity tends to decrease as the particle size decreases since large particles will not pack as compact as smaller particles. On the other hand, the surface area of the reactants increase, which will increase the reaction rate. The results for both hydration and dehydration indicate that for the same layer thickness, the effect of particle size is neglect able. This observation indicates that the two processes (increase surface area, lower layer porosity) cancel each other out.
The layer thickness does play an important role, indicating that diffusion of water vapor through a layer is rate determining for both dehydration and hydration processes.

## 2.2 Experiments performed by Netzsch Application Laboratory

The STA and DSC experiments at ECN were performed under $N_2$+$H_2O$ atmosphere, which was created by mixing dry nitrogen protective gas and water saturated nitrogen purge gas inside the machines. The relative humidity was measured at the exit of the STA machine and indicated a RH=40% at 25 °C (or $P_{H2O}$= 1.3 kPa). The actual local partial water vapor pressure near the sample surface could not be determined. So far it was assumed that this local partial water vapor pressure is equal to the value determined at the exit of the machine. However, incomplete mixing of both gas flows can result in different local partial water vapor pressures. Furthermore, since the gas flows were not continuously monitored and controlled, an undetected change in the gas flow can occur, which can change the relative humidity. Since the partial water vapor pressure is an important parameter during hydration (see also section 2.1.3.2), it is expected that a change in the partial water vapor pressure will influence the hydration process.
Netzsch Application Laboratory can perform experiments under preset and controlled $N_2$+$H_2O$ atmosphere (see above). To check if the measurements at ECN were indeed performed at $P_{H2O}$=1.3 kPa (R.H. = 40% at 25°C), it was decided to ask Netzsch Application Laboratory to repeat some experiments. The experiments were performed under the following conditions:

| Experimental conditions | |
|---|---|
| Sample carrier | TG-DSC |
| Crucibles | Platinum with pierced lids |
| Sample thermocouple | Type S |
| Atmosphere | R.H. = 40% (at 25°) $P_{H2O}$=1.3kPa<br>R.H. = 50% (at 30°)* $P_{H2O}$=2.1kPa |
| Temperature program<br>(dehydration followed by hydration) | <u>Dehydration</u><br>25 °C for 15 minutes<br>25° to 300°C with 1°C/min<br>300°C for 15 minutes<br>300° to 25°C with -5°C/min<br><u>Hydration</u><br>25 °C for 20 hours |
| Sample mass | ~10 mg |
| Calibration standard | Sapphire |

* = see text for details

Table 11: Experimental conditions for measurements performed by Netzsch Application Laboratory

### 2.2.1 Dehydration of the material

Figure 19 shows the TG curves for dehydration of magnesium sulfate measured by Netzsch Application Laboratory (‘Merck’ and ‘VWR’ in Figure 19) in comparison with the one measured at ECN.

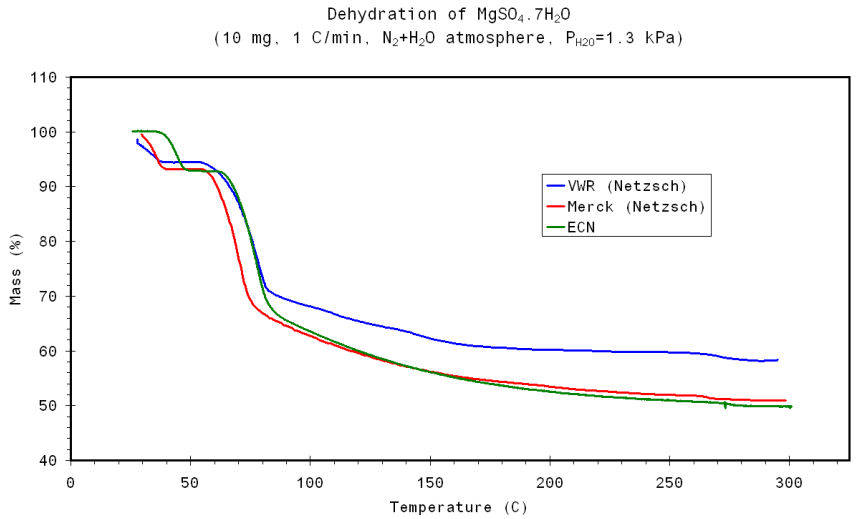


Figure 19: Experimental TG curves for dehydration of magnesium sulfate. The TG curve for material from Merck and VWR were measured by Netzsch Application Laboratory, the other was measured at ECN.

The shape of the TG curves measured by Netzsch Application Laboratory is consistent with the shape of the TG curve measured at ECN. However, the curves show that for each measurement a different final mass is achieved. Since the TG-DSC measurements and X-ray diffraction measurements at ECN show that material is completely dehydrated at 300°C, we assume that this is also the case for the measurements performed by Netzsch Application Laboratory. Together with the total mass difference, we can calculate the composition of starting material[H] . Table 12 shows the results of these calculations:

| | Amount of water molecules in starting material (R.H. = 40% at 25°C or $P_{H2O}$=1.3 kPa) | Amount of water molecules in starting material (R.H. = 50% at 30°C or $P_{H2O}$=2.1 kPa) |
|---|---|---|
| Merck | 6.3 ± 0.3 | 6.4 ± 0.3 |
| VWR | 4.5 ± 0.2 | 5.2 ± 0.2 |

Table 12: Calculated amount of water molecules in starting material at the beginning of the heating segment for experiments performed by Netzsch Application Laboratory

The results in the above Table show that the starting composition of the material from Merck is a higher hydrate than the one for the material from VWR. The composition of the starting material from VWR shows a lower hydrate than $MgSO_4.6H_2O$, which seem to dehydrate faster (from the original composition of $MgSO_4.7H_2O$) than the material from Merck. A possible explanation is that $MgSO_4.H_2O$ instead of $MgSO_4.6H_2O$ is the stable species for the vapor pressure and temperature used during the storing of the material. This would mean that the material is slowly converting to $MgSO_4.H_2O$ and forms a mixture with an overall molecular formula of $MgSO_4.5H_2O$.
Figure 20 shows the experimental TG-DSC curve for dehydration of magnesium sulfate from Merck. Please note that in the Figure below, the exothermic behavior is plotted downward in contrast to for example Figure 3):

[H] If we assume that $MgSO_4$ is the final product at T=300°C and that the initial material consists of $MgSO_4.xH_2O$, where x is the amount of water molecules in the crystal structure, we can calculate the starting material as follows:
$\frac{x \cdot M_{H2O}}{\left(M_{MgSO4} + x \cdot M_{H2O}\right)} = \frac{Mass\_decreas(\%)}{100\%}$, where Mass_decreas (%) is the total observed mass decrease and $M_{MgSO4}$ and $M_{H2O}$ are molar masses of $MgSO_4$ and water, respectively. Since x is the only unknown in the equation, it should be possible to calculate the initial composition.

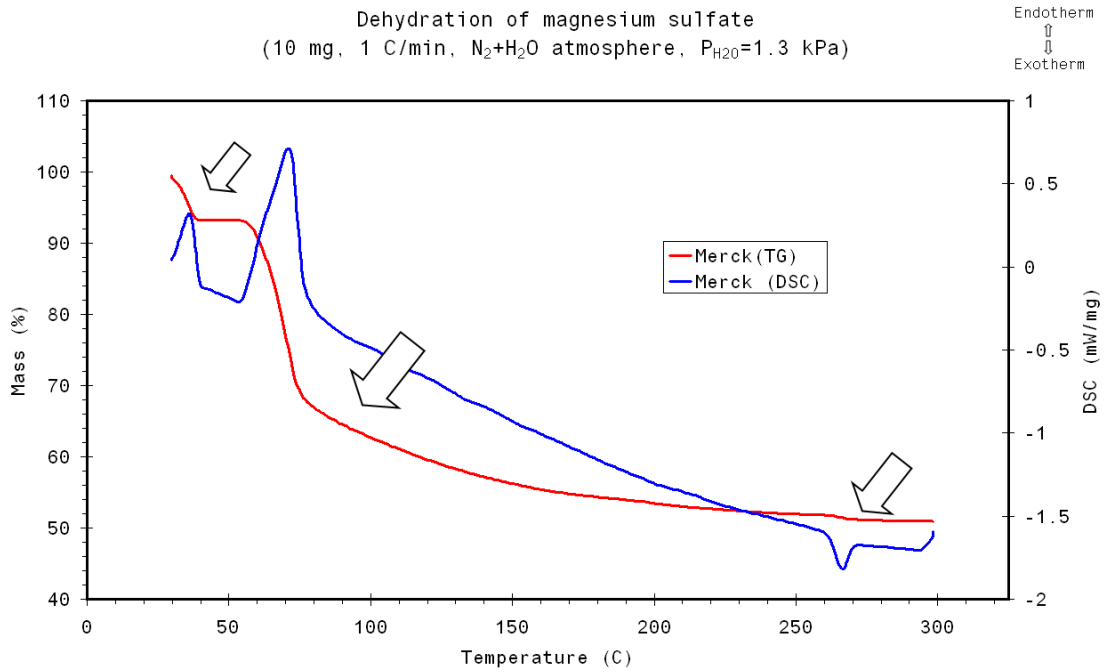


Figure 20: Experimental TG-DSC dehydration curve for magnesium sulfate for material from Merck. The particle size distribution was 38-100 µm. Arrows indicate the three dehydration steps.

The three dehydration reactions which were observed during the TG-DSC measurements performed at ECN (see Figure 4) can also be seen in the above TG-DSC dehydration curve. Since the material from VWR consists of lower hydrates (<$MgSO_4.6H_2O$), then only the second and third dehydration reactions could be identified for material from VWR (not shown) and for this reason only the TG-DSC curve for material from Merck was shown. Table 13 shows the energy densities for the three dehydration steps:

| | | $N_2+H_2O$ atmosphere | | | | |
|---|---|---|---|---|---|---|
| | | $P_{H2O}$=1.3 kPa and 25°C | | | $P_{H2O}$=2.1 kPa and 25°C | |
| Step | Conversion | Netzsch | | ECN* | Netzsch | |
| | | Merck | VWR | | Merck | VWR |
| 1 | $MgSO_4.7H_2O$ to $MgSO_4.6H_2O$ | 0.5 | -- | 0.3 | 0.6 | -- |
| 2 | $MgSO_4.6H_2O$ to $MgSO_4.0,1H_2O$ | 2.8 | 1.9 | 2.2 | 1.9 | 2.1 |
| 3 | $MgSO_4.0,1H_2O$ to $MgSO_4$ | -0.1 | $3x10^{-2}$ | -0.1 | -0.1 | -0.1 |

* = here a nitrogen-water atmosphere with $p_{H2O}$=1.3 kPa was assumed

Table 13: Average energy densities ($GJ/m^3$) determined for each dehydration step.

The results in Table 13 show that the energy density for the first and third dehydration step determined by Netzsch Application Laboratory are in agreement with the values found at ECN. The only exception is the value for the first dehydration step for material from VWR at $P_{H2O}$=1.3 kPa and 25°C, which is caused by the fact that the starting material consists of $MgSO_4.5H_2O$ instead of $MgSO_4.6H_2O$. The energy density for the second dehydration reaction varies between 1.9 and 2.8 $GJ/m^3$. Two factors are determining for calculation of the reaction enthalpy from DSC curves (and consequently also the energy density): choosing the correct base line [24] and selecting the start and end point of the reaction. From Figure 20 it can be seen that the baseline for the measurements performed at Netzsch Application Laboratory for the material from Merck is non-constant (see also Appendix F). This means that the start and end of the reaction and the shape of the baseline has to be estimated, and this will cause an additional uncertainty in the determination of the reaction enthalpy. Nevertheless, the average value of

2.4±0.3 GJ/m$^3$ (95% confidence limit) is in excellent agreement with the theoretical value of 2.5 GJ/m$^3$ [17][I].

### 2.2.2 Water uptake of the dehydrated material at different temperatures and relative humidities

#### 2.2.2.1 Water uptake of the dehydrated material at 25°C and RH=40% or $P_{H2O}$=1.3 kPa

Figure 21 shows the experimental TG-curves for hydration of dehydration material for material from Merck and VWR at 25°C and RH=40% ($P_{H2O}$=1.3 kPa)

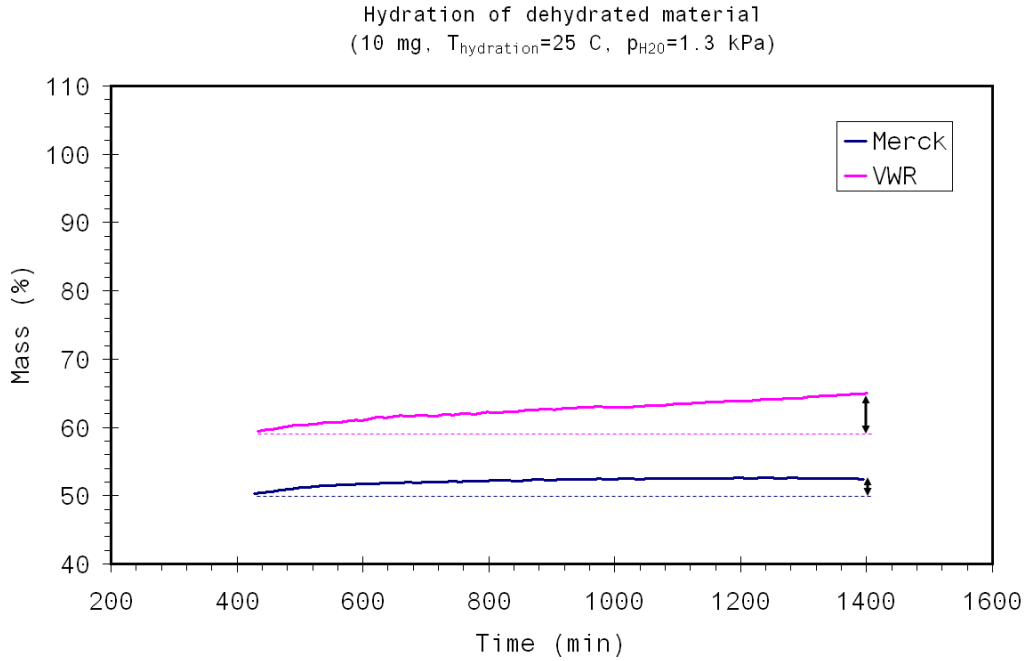


Figure 21: Experimental TG curves for hydration of dehydrated material at 25°C and $P_{H2O}$=1.3 kPa. The arrows indicate the mass change.

The results in the above Figure show that the mass of the dehydrated material only slightly increases during the 20 hours of hydration. Based on the mass change, the amount of water taken up by the material from Merck is:

$$MgSO_4(s) + 0{,}3H_2O \rightarrow MgSO_4.0{,}3H_2O\ (s) \qquad (R.8)$$

And for the material from VWR:

$$MgSO_4(s) + 0{,}8H_2O \rightarrow MgSO_4.0{,}8H_2O\ (s) \qquad (R.9)$$

The amount of water taken up by both materials is very small. Nevertheless we can observe the same trend as was seen during the experiments performed at ECN: less water is taken up by the material from Merck compared to the material from VWR (see for example Figure 11).

[I] From Table 3 we find for the second dehydration reaction $\Delta_rH$ = 57.7 kJ/mol $H_2O$ = 57.7*5.9 water molecules = 340.7 kJ/mol. The energy density is calculated as follows: Energy density = $\frac{340.7 * \rho_{MgSO4.7H2O}}{M_{MgSO4.6H2O}} = \frac{340.7 \bullet 1680}{10^9 \bullet 228.5} = 2.5\frac{GJ}{m^3}$, where $M_{MgSO4.6H2O}$ is the molar mass of $MgSO_4.6H_2O$ and $\rho_{MgSO4.7H2O}$ is the density of $MgSO_4.7H_2O$, which was taken as reference point [2]

As mentioned in the Introduction, there are four stable hydrates in the magnesium sulfate-water system: $MgSO_4$, $MgSO_4.H_2O$, $MgSO_4.6H_2O$ and $MgSO_4.7H_2O$ [11]. Since 0.3-0.8 water molecules were taken up by the material after complete dehydration, it seems to suggest that the stable hydrate at T=25°C and RH=40% ($P_{H2O}$=1.3 kPa) is $MgSO_4.H_2O$.
The results in Figure 21 are completely different from the results shown in Figure 11; clearly, the measurements at ECN were not performed at $P_{H2O}$=1.3 kPa (25°C) near the sample. Unfortunately, Netzsch Application Laboratory was unable to determine the amount of heat released during the hydration reaction from the DSC curves. However, based on the trends observed during the measurements performed at ECN it is expected that the slow uptake of small amounts of water will not result in a large (or detectable) power output.

#### 2.2.2.2 Water uptake of the dehydrated material at 25°C and RH=50% (30°C) or $P_{H2O}$=2.1 kPa

In order to obtain a larger water uptake, it was decided to perform experiments using a $N_2$+$H_2O$ atmosphere at 30°C and R.H.=50%, which corresponds to $P_{H2O}$=2.1 kPa. The results of these measurements are shown in Figure 22:

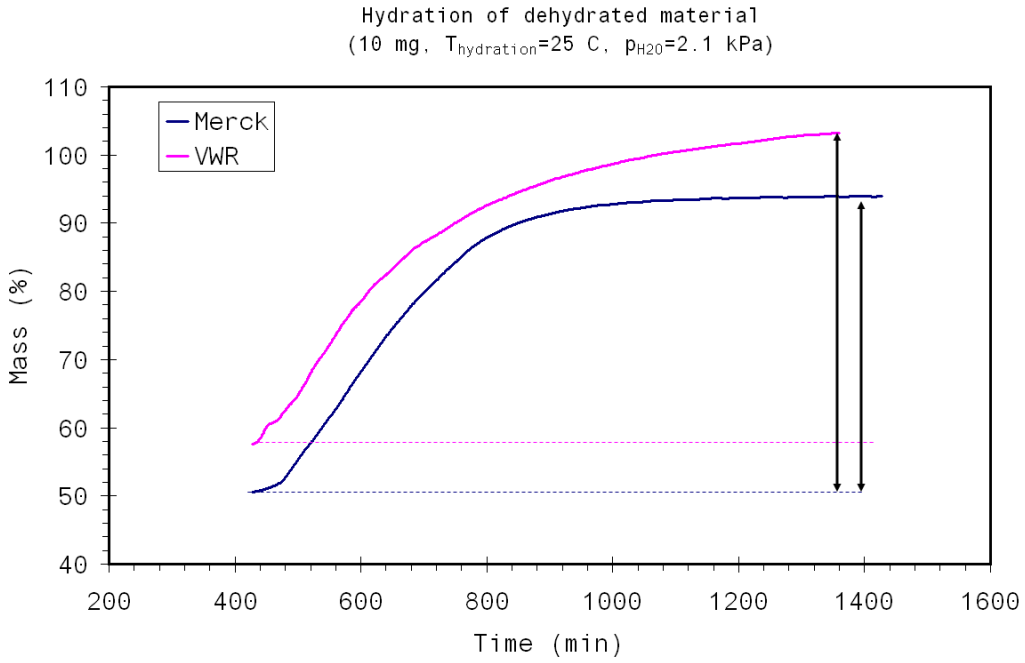


Figure 22: Experimental TG curves for hydration of dehydrated material at 25°C and $P_{H2O}$=2.1 kPa. The arrows indicate the mass change.

As can be seen from the above Figure, the samples showed a larger and faster mass increase, which corresponds to the following hydration reaction for material from Merck:

$$MgSO_4(s) + 5{,}7H_2O \rightarrow MgSO_4.5{,}7H_2O\ (s) \qquad (R.10)$$

And for the material from VWR:

$$MgSO_4(s) + 5{,}3H_2O \rightarrow MgSO_4.5{,}3H_2O\ (s) \qquad (R.11)$$

The amount of water taken up during hydration is almost equal for both materials. This result was not expected, since results so far indicated a slower water uptake by the material from Merck. So far we have no adequate explanation for this behavior (under investigation).

The results shown in Figure 22 resemble the results shown in Figure 11, which suggests that the partial water vapor pressure that was used during the experiments at ECN is closer to 2.1 kPa than 1.3 kPa (see also Figure 21). The hydration reactions stated above suggest that under the experimental conditions used during these experiments (RH=50% at 30°C), $MgSO_4.6H_2O$ is most likely stable species. Again, Netzsch Application Laboratory was unable to determine the heat release during hydration. But we expect a larger power output during these hydration reactions compared to the result acquired at T=25°C and RH=40% ($P_{H2O}$=1.3 kPa) due to larger amount of water taken up during hydration.

### 2.2.3 Water uptake of the dehydrated material at 50°C

Until now, the dehydrated material was allowed to take up water at 25°C. In practical conditions, the material should be able to take up water (and release heat) at temperatures ≥40°C (see also Introduction). For this reason it was decided to measure the water take up of dehydrated material at 50°C. The experiments were performed at $P_{H2O}$=2.1 kPa (RH=50% at 30°C), since the water take up for this partial water vapor pressure was the largest (see previous section). The result of this experiment is shown in Figure 23:

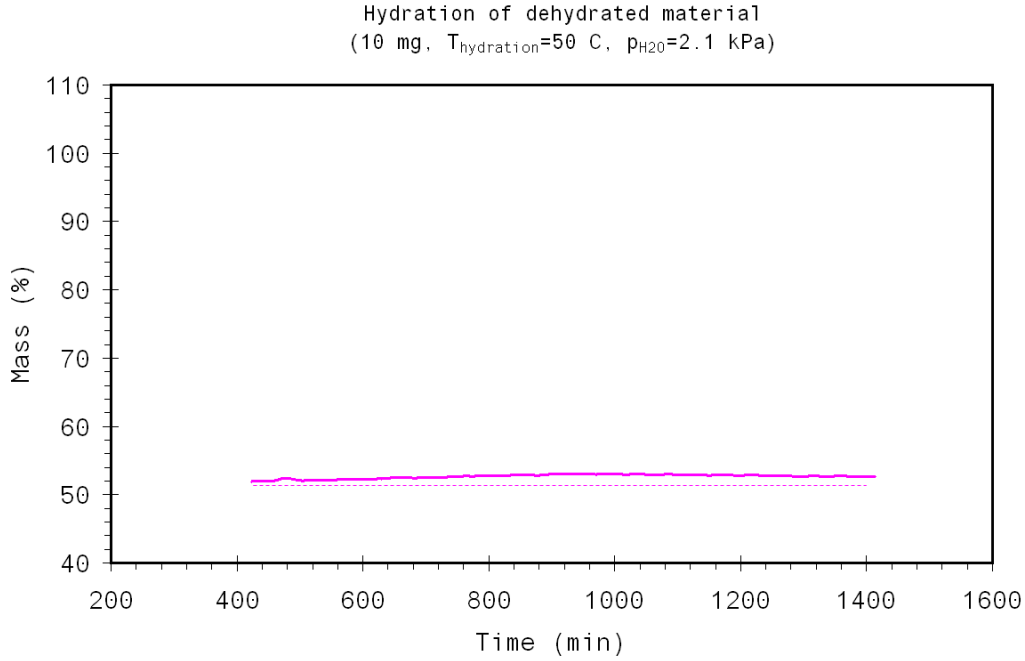


Figure 23: Experimental TG curves for hydration of dehydrated material from VWR at 50°C and $P_{H2O}$=2.1 kPa

The results in the above Figure clearly indicate that almost no water taken up by the material. It seems that under these experimental conditions (T=50°C and $P_{H2O}$=2.1 kPa) $MgSO_4$ is the final product. Thus, even at higher water vapor pressure, which is favorable for the water uptake by $MgSO_4$ (see above), the material is unable to take up water. This means that under practical conditions the water uptake by $MgSO_4$ is problematic.

### 2.2.4 Magnesium sulfate – water equilibriums

In the previous sections it was observed that the final product of hydration depends on the temperature and partial water vapor pressure. Table 14 gives a summary of the observations discussed in the previous sections:

| | Partial water vapor pressure | |
|---|---|---|
| Temperature | 1.3 kPa | 2.1 kPa |
| 25°C | $MgSO_4.H_2O$ (R.H.=40%) | $MgSO_4.6H_2O$ (R.H.=67%) |
| 50°C | -- | $MgSO_4$ (R.H.=17%) |

Table 14: Stable species observed after 20 hours hydration of $MgSO_4$

Figure 24 shows the temperature- relative humidity relations in the magnesium sulfate- water system (1 atm.) from Chou et al [10] together with the results from Table 14:

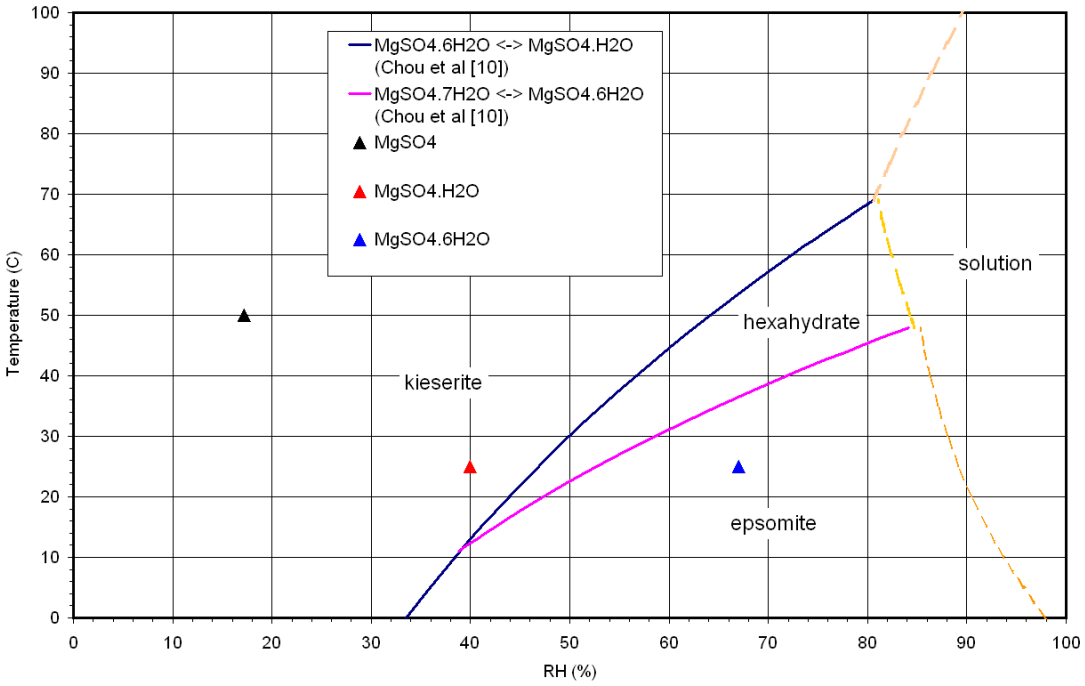


Figure 24: Temperature – relative humidity relations in the system $MgSO_4$-$H_2O$ at 1 atm. The lines were taken from Chou et al [10]. The triangles are experimental results and denote the final product after 20 hours hydration of $MgSO_4$.

The lines in the above Figure were taken from Chou et al [10], who experimentally determined the $MgSO_4.7H_2O$ (Epsomite) – $MgSO_4.6H_2O$ (hexahydrate) equilibrium. An elaborate study by Chipera et al [11] confirms the position of this equilibrium line. Chou et al [10] estimated the equilibrium between $MgSO_4.6H_2O$ and $MgSO_4.H_2O$ (kieserite) based on thermodynamic data, and indicates that there is some uncertainty in the position of this equilibrium. This has also been confirmed by Chipera et al [11], who shows that the position of this equilibrium line is questionable. Despite this uncertainty, it was decided to show the hexahydrate-kieserite equilibrium line in Figure 24, since it illustrates that the conversion from lower hydrates (e.g. kieserite) to higher hydrates (hexahydrate/Epsomite) occurs at high relative humidity. This was also found by Chipera et al [11].

Figure 24 includes the experimental results discussed in the previous sections. The results indicate that the final product after hydration at T=25°C and $P_{H2O}$=2.1 kPa (RH=67%) is most likely not $MgSO_4.6H_2O$ but $MgSO_4.7H_2O$, indicating that the uptake of the last water molecule under these conditions is quite slow. The formation of $MgSO_4.H_2O$ at T=25°C and $P_{H2O}$=1.3 kPa (RH=40%) is in agreement with the results from Chou et al [10]. At T=50°C and $P_{H2O}$=2.1 kPa (RH=17%) it was observed that no water was taken up by the $MgSO_4$. This could mean that there is an addition equilibrium line between kieserite ($MgSO_4.H_2O$) and $MgSO_4$. Figure 24 indicates that the position of this equilibrium line should be at low relative humidity's, which was also suggested by Chipera et al [11].

## 2.3 Cyclability of the material

An important requirement for the usage of magnesium sulfate as seasonal storage is that the reversible reaction can be used a several times (=cyclability). A cyclability experiment can be performed using the STA machine at ECN. However, the sample sizes used during these experiments are very small (few milligrams), while in practice the amount of material will be more in the order of several kilograms. For this reason it was decided to perform experiments using 17 grams of material with a particles of 38-106 micron. A Petri dish, with an internal diameter of 7 cm, served as a container in which the material was placed. The layer thickness of the sample was approximately 0.8 cm.
The samples were placed in an oven and heated up from room temperature to 150°C with 1°C/min. Thermocouple measurements inside the oven show that the temperature is distributed uniformly in the oven. After an isothermal period of 15 minutes at 150°C, the samples were cooled down to T=20°C and placed outside the oven, allowing hydration to laboratory air (T=20°C and RH=70% or $P_{H2O}$ = 1.6 kPa) for 20 hours. The dehydration-hydration procedure was repeated two times. The relative humidity and the temperature in the laboratory were monitored using an Escort Junior EJ-HS-B-8 data logger. Figure 25 shows the results from these experiments.

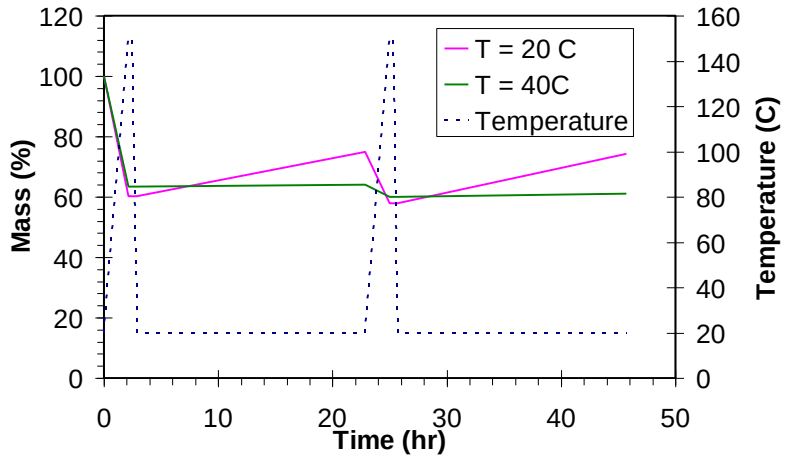


Figure 25: Experimental results of two hydration/dehydration cycles at 20°C and 40°C for the material from Merck.

An initial mass loss of ~40% is observed when the material is heated to 150°C, corresponding to a loss of ~5.5 water molecules. For hydration at 20°C, the material takes up water until 74% of the initial mass is reached. The results for hydration at 20°C indicate that magnesium sulfate can be used several times.
Figure 25 also shows the results of cyclability experiments performed at a hydration temperature of 40°C, where the dehydrated sample was placed inside an oven at 40 °C for hydration. Here too, the Escort Junior EJ-HS-B-8 data logger was used to monitor both temperature and relative humidity during hydration. The results for hydration at 40°C show no water uptake after dehydration. This can be explained by the fact that the partial water vapor pressure during these experiments is considerably lower than for cyclability experiments performed at 20°C (0.4 kPa (RH=6%) at 40°C compared to 1.6 kPa (RH=70%) at 20°C). This effect of partial water vapor pressure on hydration is in agreement with the results from the measurements by Netzsch (see previous section).
The relative humidity in the laboratory changed from day to day, depending on the weather outside. The changing humidity allows us to investigate the influence of the partial water vapor pressure on the cyclability at a hydration temperature of 20 °C. The experiments were performed for different particles sizes and three cycles were investigated. The results are shown in Figure 26:

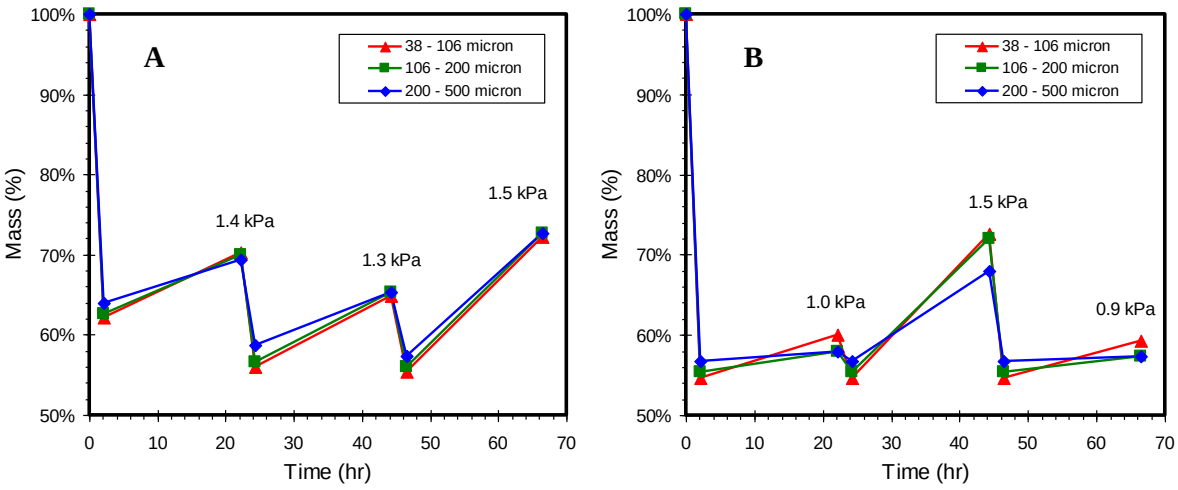


Figure 26: Experimentally determined mass changes as function of time for 15 min isothermal part at 150°C (A) and 4 hours isothermal part at 150°C (B). The samples from VWR were dehydrated in an oven and hydrated in laboratory air of 20°C. The partial water vapor pressures (in kPa) are also indicated in the above Figures.

Figure 21A shows that the mass decrease after the first dehydration is smaller than after the second dehydration. From STA measurements we would expect a 45-50% decrease at 150°C (see for example Figure 4), which is only reached after the second dehydration. This suggests that the sample isn't completely dehydrated after the first dehydration step. Therefore, experiments were performed with 4 hours (instead of 15 minutes) isothermal part at 150°C. The results of these experiments are shown in Figure 26B. Clearly, increasing the time of the isothermal part results in a constant final mass after dehydration which shows a good correspondence to the results obtained from STA measurements: in both cases a ~55% of the initial mass was left after dehydration.

After hydration, the actual increased mass is strongly dependent on the partial water vapor pressure of the environment. In general, higher partial water vapor pressure leads to higher mass increase. The effect of particle size (porosity) on the cycling behavior is only marginal in correspondence to the results obtained with STA machine.

## 2.4 Summary and conclusions

The dehydration and hydration processes in the magnesium sulfate-water system were investigated using thermal analysis (at ECN and by Netzsch Application Laboratory), X-ray diffraction, particle distribution measurements and SEM-EDX. The results show that the dehydration of $MgSO_4.7H_2O$ proceeds in three steps:

1. $MgSO_4.7H_2O\ (s) \Rightarrow MgSO_4.6H_2O\ (s) + H_2O\ (g)$ at 25-55°C
2. $MgSO_4.6H_2O\ (s) \Rightarrow MgSO_4.0{,}1H_2O\ (s) + 5{,}9H_2O\ (g)$ at 60-265°C
3. $MgSO_4.0{,}1H_2O\ (s) \Rightarrow MgSO_4\ (s) + 0{,}1H_2O(g)$ at ~275°C

Experimental X-ray diffraction patterns confirm that the material is completely dehydrated at 300°C. Melting of $MgSO_4.7H_2O$ was observed during the first dehydration step; the experimentally determined melting temperature of 52°C is in good agreement with values found in literature [5, 13].

The second dehydration step is most interesting for compact seasonal solar heat storage, because of large energy density (2.2±0.1 GJ/m$^3$) and the fact that the reaction occurs in a temperature range that can be covered by solar collectors ( ≤150°C). The TG-DSC measurements indicate that this dehydration step is combination of several dehydration steps. X-ray diffraction experiments indicated the second dehydration step involves a material structure change from crystalline ($MgSO_4.6H_2O$) to an amorphous phase until crystalline $MgSO_4$ is formed. The X-ray diffraction results further suggest that $MgSO_4.3H_2O$ is formed at T=100°C as intermediate during this second dehydration step.

The kinetics of the second dehydration step can be best described by a three-step consecutive reaction, where the first two reaction steps are 1$^{st}$ order and the last reaction step is 4$^{th}$ order.

The partial water vapor pressure which was used during the STA/DSC measurements at ECN was estimated to be $P_{H2O}$=1.3kPa. However, measurements performed by Netzsch Application Laboratory revealed that the partial water vapor pressure during the measurement at ECN is actually higher and probably closer to 2.1 kPa.

The water uptake of the dehydrated material strongly depends on the temperature and the partial water vapor pressure. The results show that higher magnesium sulfate hydrates can only be formed from $MgSO_4$ at T=25°C and $p_{H2O}$=2.1 kPa. The energy density of this singe step hydration reaction is 2.1 GJ/m$^3$, which shows that energy can be stored and retrieved using magnesium sulfate hydrates. At lower partial water vapor pressure (1.3 kPa) or higher temperature (50°C), it was observed that there was no or marginal water uptake. This means that the application of magnesium sulfate as thermochemical material for seasonal heat storage is quite problematic.

A first kinetic evaluation of the hydration reaction reveals that the kinetics of the hydration from $MgSO_4$ to $MgSO_4.5{,}6H_2O$ can be best described by an single step Avrami-Erofeev (nucleation) model. However, the kinetics were determined at a single temperature and partial water vapor pressure and for more accurate and complete kinetic evaluation of hydration reaction it is recommended to evaluate data at different temperatures and (controlled) different partial water vapor pressures.

In general, the hydration and dehydration rate was only effect by a change in layer thickness, and not by changing the particle diameter (layer porosity), indicating that diffusion of mass and heat plays an important role in the dehydration and hydration processes.

An oven was used to investigate the cyclability of the material. The material shows a good cyclability at 20°C (and $P_{H2O}$ = 1.6 kPa) but the material is unable to take up at 40°C.

Material from two suppliers (VWR and Merck) were evaluated and it was discovered that the hydration was slower for the material from Merck than for VWR. So far, only a difference in stress within the crystal structure was detected using X-ray diffraction.

## 2.5 References


1. Lahmidi, H., Mauran, S. and Goetz V., "Definition, test and simulation of a thermochemical storage process adapted to solar thermal systems", Sol. Energy 80, 883-893 (2006).
2. Visscher, K. Veldhuis, J.B.J., Oonk, H.A.J., van Ekeren, P.J. and Blok, J.G.,. (2004) ECN Report ECN-C—04-074: *Compacte chemische seizoenopslag van zonnewarmte; Eindrapportage*, ECN, Petten
3. Ruiz-Agudo, E., Martin-Ramos, J.D., and Rodriguez-Navarro, C., "*Mechanism and kinetics of dehydration of Epsomite crystals formed in the presence of organic additives"*, J.Phys.Chem. B. **111**, 41-52 (2007)
4. Zondag, H., Essen, V.M. van, He, Z., Schuitema, R. and Helden, W. van, "*Characterization of MgSO4 for thermochemical storage*", in Second International Renewable Energy Storage Conference (IRES II), Bonn, Germany (2007)
5. Emons, H.H., Ziegenbalf, G., Naumann, R. and Paulik, F.,"*Thermal decomposition of the magnesium sulfate hydrates under quasi-isothermal and quasi-isobaric conditions"*, J. Therm. Anal. **36**, 1265-1279 (1990)
6. Heide,K., "*Thermochemische und Kinetische Untersuchungen der Endothermen Umbildungsreaktionen de Epsomits (MgSO4.7H2O)*", J. Therm. Anal. **1**, 183-194 (1969)
7. Hamad, S. El D., "*An experimental study of salt hydrate MgSO4.7H2O*", Therm. Acta **13**, 409-418 (1975)
8. Phadnis, A.B, and Deshpande, V.V., "*On the dehydration of MgSO4.7H2O*", Therm. Acta **43**, 249-250 (1981)
9. Paulik, J., Paulik, F., and Arnold, M., "*Dehydration of magnesium sulfate heptahydrate investigated by quasi isothermal-quasi isobaric TG",* Therm. Acta **50**, 105-110 (1981)
10. Chou, M.I., and Seal II, R.R., "*Evaporites, Water and Life, Part I: Determination of Epsomite-Hexahydrate Equilibria by the Humidity-Buffer Technique at 0.1 MPa with Implications for Phase Equilibria in the System MgSO4-H2O*", Astrobiology **3**, 619-630 (2003)
11. Chipera, S.J. and Vaniman, D.T. "*Experimental stability of magnesium sulfate hydrates that may be present on Mars*", Geochim. Cosmochim. Acta **71**, 241-250 (2007)
12. Vaniman, D.T., Bish, D.L., Chipera, S.L., Fialips, C.L., Carey, J.W., and Feldman, W.C., "*Magnesium sulfate salts and the history of water on Mars*", Nature **431**, 663-665 (2004)
13. Van der Voort, I.M., "*Characterization of a thermal chemical material storage*", Eindhoven University of Technology, 2007
14. PDF crystallographic database, JCPDS-ICDD, 1997. JCPDS-ICDD Powder Diffraction File (PDF-2), International Centre for Diffraction Data, 12 Campus Boulevard, Newtown Square, PA 19073-3273 USA, PHONE: 610-325-9814, FAX: 610-325-9823, info@icdd.com, 1997
15. Steiger, M., and Linnow, K., "*Hydration of MgSO4.H2O and Generation of Stress in Porous Materials*", Crystal Growth and Design **8**, 336-343
16. Atkins, P., and De Paula, J., "*Atkins'Physical Chemistry" (Oxford University Press, Oxford, 2006)*
17. Wagman, D. D., Evans, W. H., Parker, V. B., Schumm, R. H. and Halow, I.., "*The NBS tables of chemical thermodynamic properties: selected values for inorganic and C1 and C2 organic substances in SI units*", J. Phys. Chem. Ref. Data **11** (1982).
18. House, J.E., *Principles of Chemical Kinetics, second edition* (Elsevier Inc., London, 2007)
19. Vyazovkin, S.V., and Lesnikovich, A.I., "*Estimation of the pre-exponential factor in the isoconversional calculation of effective kinetic parameters*", Therm. Acta **128** 297-300 (1988)

20. Vyazovkin, S.V., and Dollimore, D., "*Linear and nonlinear procedures in Isoconversional computation of the activation energy of nonisothermal reactions in solids*", J. Chem. Inf. Comput. Sci. **36** 42-45 (1996)
21. Vyazovkin, S.V., and Wight, C.A., "*Model-free and model-fitting approaches to kinetic analysis of isothermal and nonisothermal data*", Therm. Acta **340-341** 53-68 (1999)
22. http://www.therm-soft.com/english/kinetics.htm
23. Opfermann, J., "*Kinetic analysis using multivariate non-linear regression*", J. Therm. Anal. Cal. **60**, 641-658 (2000)
24. Thermal analysis: Information for users, USERCOM 25, http://us.mt.com/mt/ed/userCom/TA_UserCom25_Editorial-Generic_1201692194205.jsp
25. Berendsen, H.J.C, *"Goed meten met Fouten",*Uitg.Bibli.der RU, Groningen , 1997 (in Dutch)
26. Goetz, V. and Marty, A., "*A model for reversible solid-gas reactions submitted to temperature and pressure constrains: simulation of the rate of reaction in solid-gas reactor used as chemical heat pump*", Chem. Eng. Sci. **47**, 4445-4454 (1992)
27. Zondag, H.A., "*WAELS C inventory on separate TCM reactor design options for closed TCM seasonal storage systems*", ECN-Memo

# Appendix A EDX results for starting material from Merck and VWR

```
Fri Aug 15 14:00:37 2008

VWR-1

Filter Fit Method
Chi-sqd = 7.86     Livetime = 60.0 Sec.
Standardless Analysis
Element   Relative     Error        Net      Error
          k-ratio    (1-Sigma)     Counts  (1-Sigma)
  C -K       ---         ---         604 +/-    52
  O -K    0.44742 +/- 0.00428      14955 +/-   143
  Mg-K    0.19605 +/- 0.00174      18371 +/-   163
  Pt-M       ---         ---        2439 +/-   312
  S -K    0.35653 +/- 0.00412      27547 +/-   318

Adjustment Factors           K           L           M
  Z-Balance:              0.00000     0.00000     0.00000
  Shell:                  1.00000     1.00000     1.00000

PROZA Correction  Acc.Volt.= 15 kV  Take-off Angle=35.61 deg
Number of Iterations = 7

Element  k-ratio    ZAF   Atom %  Element  Wt % Err.
         (calc.)                    Wt %   (1-Sigma)
  O -K    0.2521   2.313   71.17   58.30    +/- 0.56
  Mg-K    0.1105   1.596   14.16   17.62    +/- 0.16
  S -K    0.2009   1.198   14.66   24.07    +/- 0.28
  Total                   100.00  100.00

   The number of cation results are based upon 24 Oxygen atoms
```

Fri Aug 15 14:17:56 2008

VWR-2

Filter Fit Method
Chi-sqd = 6.07  Livetime = 60.0 Sec.
Standardless Analysis

| Element | Relative k-ratio | Error (1-Sigma) | Net Counts | Error (1-Sigma) |
|---|---|---|---|---|
| C -K | --- | --- | 783 | +/- 50 |
| O -K | 0.40178 | +/- 0.00477 | 10104 | +/- 120 |
| Mg-K | 0.20328 | +/- 0.00200 | 14332 | +/- 141 |
| Pt-M | --- | --- | 1757 | +/- 282 |
| S -K | 0.39494 | +/- 0.00497 | 22961 | +/- 289 |

| Adjustment Factors | K | L | M |
|---|---|---|---|
| Z-Balance: | 0.00000 | 0.00000 | 0.00000 |
| Shell: | 1.00000 | 1.00000 | 1.00000 |

PROZA Correction  Acc.Volt.= 15 kV  Take-off Angle=35.61 deg
Number of Iterations = 7

| Element | k-ratio (calc.) | ZAF | Atom % | Element Wt % | Wt % Err. (1-Sigma) |
|---|---|---|---|---|---|
| O -K | 0.2267 | 2.444 | 68.78 | 55.39 | +/- 0.66 |
| Mg-K | 0.1147 | 1.572 | 14.73 | 18.02 | +/- 0.18 |
| S -K | 0.2228 | 1.193 | 16.48 | 26.59 | +/- 0.33 |
| Total | | | 100.00 | 100.00 | |

The number of cation results are based upon 24 Oxygen atoms

Merck-1

Refit _C -K' _C -K"
Refit _Pt-M" _S -K"
Filter Fit Method
Chi-sqd = 5.61  Livetime = 60.0 Sec.
Standardless Analysis

| Element | Relative k-ratio | Error (1-Sigma) | Net Counts | Error (1-Sigma) |
|---|---|---|---|---|
| C -K | --- | --- | 154 | +/- 22 |
| O -K | 0.42145 | +/- 0.00482 | 8665 | +/- 99 |
| Mg-K | 0.19299 | +/- 0.00215 | 11123 | +/- 124 |
| Pt-M | --- | --- | 1684 | +/- 107 |
| S -K | 0.38556 | +/- 0.00328 | 18323 | +/- 156 |

| Adjustment Factors | K | L | M |
|---|---|---|---|
| Z-Balance: | 0.00000 | 0.00000 | 0.00000 |
| Shell: | 1.00000 | 1.00000 | 1.00000 |

PROZA Correction  Acc.Volt.= 15 kV  Take-off Angle=35.61 deg
Number of Iterations = 7

| Element | k-ratio (calc.) | ZAF | Atom % | Element Wt % | Wt % Err. (1-Sigma) |
|---|---|---|---|---|---|
| O -K | 0.2373 | 2.397 | 70.09 | 56.87 | +/- 0.65 |
| Mg-K | 0.1087 | 1.585 | 13.98 | 17.23 | +/- 0.19 |
| S -K | 0.2171 | 1.193 | 15.93 | 25.90 | +/- 0.22 |
| Total | | | 100.00 | 100.00 | |

The number of cation results are based upon 24 Oxygen atoms

Fri Aug 15 14:25:54 2008

Merck-2

Filter Fit Method
Chi-sqd = 5.22  Livetime = 60.0 Sec.
Standardless Analysis

| Element | Relative k-ratio | Error (1-Sigma) | Net Counts | Error (1-Sigma) |
|---|---|---|---|---|
| C -K | --- | --- | 399 | +/- 43 |
| O -K | 0.44128 | +/- 0.00514 | 9794 | +/- 114 |
| Mg-K | 0.19713 | +/- 0.00211 | 12265 | +/- 131 |
| Pt-M | --- | --- | 1425 | +/- 256 |
| S -K | 0.36159 | +/- 0.00509 | 18551 | +/- 261 |

| Adjustment Factors | K | L | M |
|---|---|---|---|
| Z-Balance: | 0.00000 | 0.00000 | 0.00000 |
| Shell: | 1.00000 | 1.00000 | 1.00000 |

PROZA Correction  Acc.Volt.= 15 kV  Take-off Angle=35.61 deg
Number of Iterations = 7

| Element | k-ratio (calc.) | ZAF | Atom % | Element Wt % | Wt % Err. (1-Sigma) |
|---|---|---|---|---|---|
| O -K | 0.2486 | 2.330 | 70.86 | 57.92 | +/- 0.67 |
| Mg-K | 0.1111 | 1.592 | 14.24 | 17.68 | +/- 0.19 |
| S -K | 0.2037 | 1.198 | 14.90 | 24.40 | +/- 0.34 |
| Total | | | 100.00 | 100.00 | |

The number of cation results are based upon 24 Oxygen atoms

# Appendix B analysis of experimental uncertainty

In this Appendix the equations are given which were used to calculate the experimental uncertainty. Detailed information on this subject can be found in Ref [25]

## Uncertainty in dehydrated water molecules

The amount of dehydrated water molecules are determined using the following equation:

$$n_{H_2O} = \frac{\Delta m}{7.31\%} \qquad \text{(B-1)}$$

Where $n_{H_2O}$ is the total amount of dehydrated water molecules per dehydration step, Δm is the mass difference per dehydration step (%) and 7.31 % is the theoretical mass difference corresponding to one dehydrated water molecule when $MgSO_4.7H_2O$ is the starting material. The uncertainty in the amount of calculated amount of dehydrated water molecules is calculated using the following equation:

$$\sigma_{n_{H_2O}} = \left|\frac{\partial n_{H_2O}}{\partial \Delta m}\right| \cdot \sigma_{\Delta m} = \left|\frac{1}{7.31\%}\right| \cdot \sigma_{\Delta m} \qquad \text{(B-2)}$$

Where $\sigma_{n_{H_2O}}$ is the uncertainty in the calculated amount of dehydrated water molecules, $\frac{\partial n_{H_2O}}{\partial \Delta m}$ is the partial derivative calculated using equation (B-1) and $\sigma_{\Delta m}$ is the uncertainty in the mass difference per dehydration step. The value $\sigma_{n_{H_2O}}$ can be calculated based on equation (B-1) and the value of $\sigma_{\Delta m}$ (see Table 1).

## Uncertainty in reaction enthalpy per water molecule and energy storage density

The reaction enthalpy per water molecule ($\Delta_rH_{H2O}$, kJ/mol $H_2O$) is calculated using the following equation:

$$\Delta_r H_{H_2O} = \frac{\Delta_r H}{n_{H_2O,r}} \qquad \text{(B-3)}$$

Where $\Delta_rH$ is the enthalpy of reaction (kJ/mol) and $n_{H_2O},r$ is the total amount of water molecules involved in the dehydration reaction. Here it is assumed that the reaction proceeds via a fixed number of water molecules. The uncertainty in the enthalpy of reaction per water molecule ( $\sigma_{\Delta_r H_{H2O}}$ ) can be calculated using the following equation:

$$\sigma_{\Delta_r H_{H2O}} = \left|\frac{\delta \Delta_r H_{H_2O}}{\delta \Delta_r H}\right| \cdot \sigma_{\Delta_r H} = \left|\frac{1}{n_{H_2O,r}}\right| \cdot \sigma_{\Delta_r H} \qquad \text{(B-4)}$$

Where $\frac{\delta \Delta_r H_{H_2O}}{\delta \Delta_r H}$ is the partial derivative calculated using equation (B-3) and $\sigma_{\Delta_r H}$ is the uncertainty in the enthalpy of reaction.

The energy storage density ($\rho_{E,}$ GJ/m$^3$) is calculated using the following equation:

$$\rho_E = \frac{\Delta_r H \cdot \rho_{MgSO_4 \cdot 7H_2O}}{M_{MgSO_4 \cdot 7H_2O}} \qquad \text{(B-5)}$$

Where $\rho_{MgSO_4 \cdot 7H_2O}$ [kg/m$^3$] and $M_{MgSO_4 \cdot 7H_2O}$ [kg/mol] are the density and molar mass of $MgSO_4.7H_2O$, respectively. It should be noted that the enthalpy of reaction ($\Delta_r H$) in equation (B-5) is expressed in terms of GJ/mol instead of kJ/mol (see above). The uncertainty in the energy density $(\sigma_{\rho_E})$ can be calculated assuming that the error in the density and molar mass of $MgSO_4.7H_2O$ are neglect able:

$$\sigma_{\rho_E} = \left| \frac{\partial \rho_E}{\delta \Delta_r H} \right| \cdot \sigma_{\Delta_r H} = \left| \frac{\rho_{MgSO_4 \cdot 7H_2O}}{M_{MgSO_4 \cdot 7H_2O}} \right| \cdot \sigma_{\Delta_r H} \qquad \text{(B-6)}$$

## Uncertainty in calculated amount of water molecules in starting material (Table 12)

The starting composition (= amount of water molecules in the starting material) is calculated based on the total mass difference after dehydration ($\Delta$m, %):

$$\frac{n_{H_2O(start)} \cdot M_{H_2O}}{n_{H_2O(start)} \cdot M_{H_2O} + M_{MgSO_4}} \cdot 100 = \Delta m \qquad \text{(B-7)}$$

Where $n_{H_2O(start)}$ is the amount of water molecules in the starting material, $M_{H_2O}$ is the molar mass of water (g/mol) and $M_{MgSO_4}$ is the molar mass of magnesium sulfate anhydrate. Rearranging equation (B-7) leads to the following equation:

$$n_{H_2O(start)} = \frac{\Delta m \cdot M_{MgSO_4}}{M_{H_2O} \cdot 100 - \Delta m \cdot M_{H_2O}} \qquad \text{(B-8)}$$

Then the following expression can be found for calculating error in the amount of water molecules in the starting material ( $\sigma_{n_{H2O}}$ ):

$$\sigma_{N_{H2O}} = \left| \frac{\delta n_{H_2O(start)}}{\delta \Delta m} \right| \cdot \sigma_{\Delta m} = \frac{M_{MgSO_4} \cdot 100 \cdot M_{H_2O}}{\left( M_{H_2O} \cdot 100 - M_{H_2O} \cdot \Delta m \right)^2} \cdot \sigma_{\Delta m}$$

Where $\sigma_{\Delta m}$ is the uncertainty in the determination of the total mass difference. For the experiments described in this report an estimated error of 1% in the mass difference determination was used.

# Appendix C Determination of enthalpy of formation for $MgSO_4.0,1H_2O$

The NBS database [17] gives the following enthalpies of formation in the solid magnesium sulfate-water system:

| Material | Enthalpy of formation ($\Delta_r H$) kJ/mol | Amount of hydrated water molecules |
|---|---|---|
| $MgSO_4$ | -1284.9 | 0 |
| $MgSO_4.H_2O$ (crystalline) | -1602.1 | 1 |
| $MgSO_4.H_2O$ (amorphous) | -1574.9 | 1 |
| $MgSO_4.2H_2O$ | -1896.2 | 2 |
| $MgSO_4.4H_2O$ | -2496.6 | 4 |
| $MgSO_4.6H_2O$ | -3087 | 6 |
| $MgSO_4.7H_2O$ | -3388.71 | 7 |

Table C.1 Enthalpy of formation for the solid magnesium-water system taken from [17]

In the enthalpy of formation is plotted as function of the amount of dehydrated water molecules:

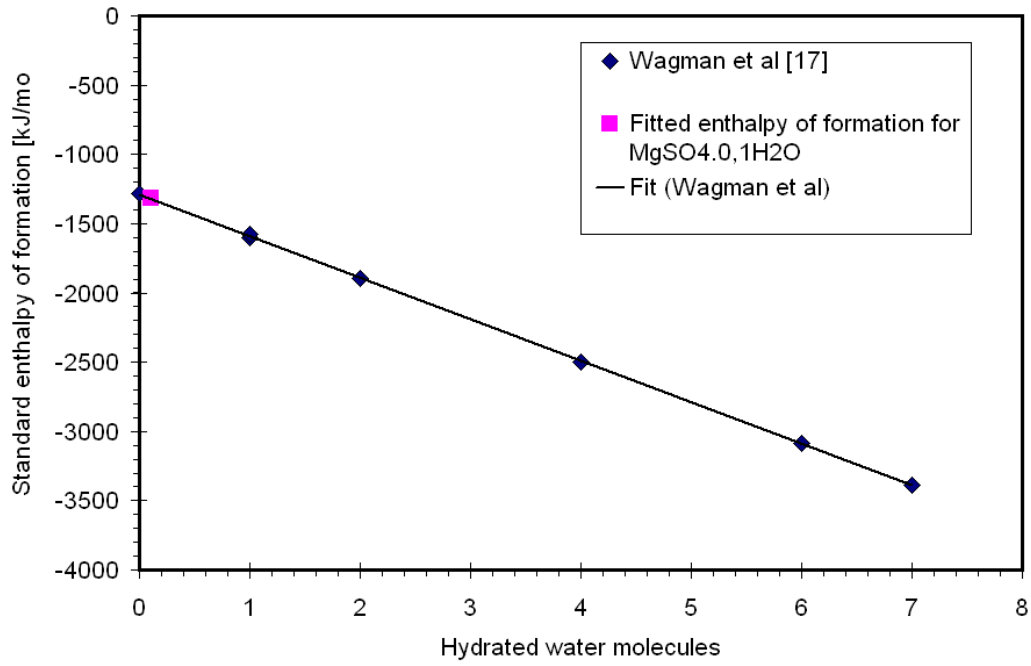


Figure C.1 Standard enthalpies of formation for hydrates of magnesium sulfate as function of the number of hydrated water molecules (0=$MgSO_4$, 7=$MgSO_4.7H_2O$) [17]

The data was fitted to a linear equation (Y=AX+B) and the following variables were determined ($R^2$ = 0.9999): A=-300.2 kJ/mol/water molecule and B=-1289.5 kJ/mol.

The enthalpy of formation for $MgSO_4.0,1H_2O$ can now be calculated using the linear equation and the fitted variables:

$\mathbf{M_{MgSO4.0,1H2O}}$=300.2*0,1 -1289.5=-1319.6 kJ per mol

# Appendix D SEM pictures

In this appendix the SEM picture before and after dehydration, and after hydration are presented. The material is dehydrated by increasing the temperature from 25°C to 150°C at 1°C/min. After cooling down to room temperature (25°C), the material is allowed to hydrated under ambient conditions (RH=50-55%).

**Merck**

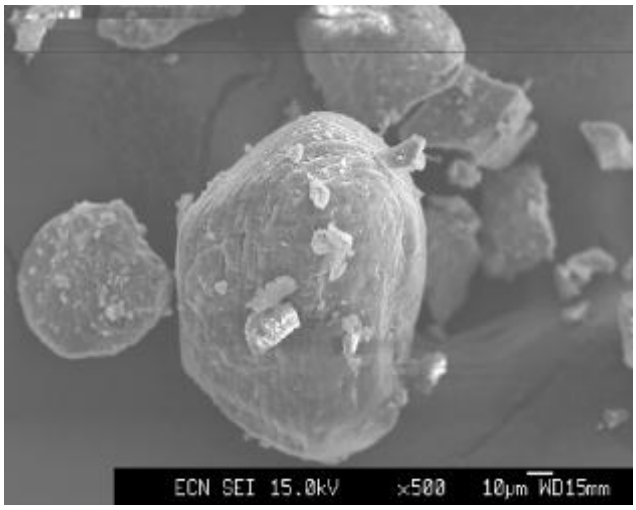


Prior to dehydration

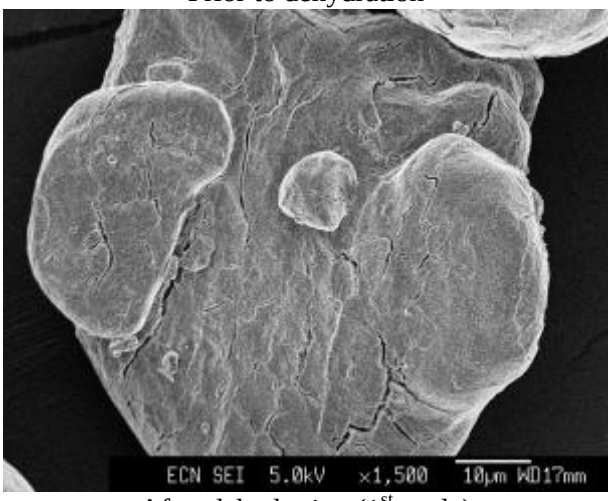


After dehydration (1st cycle)

**Prolabo**

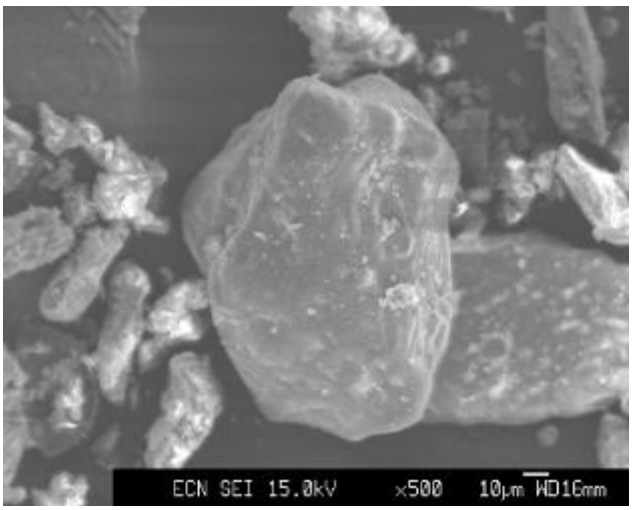


Prior to dehydration

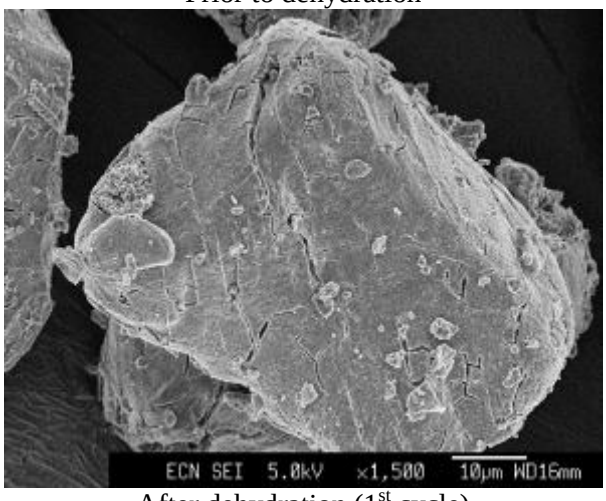


After dehydration (1st cycle)

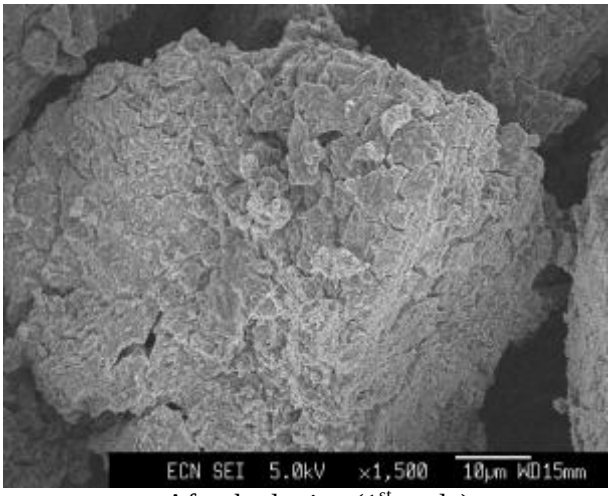

After hydration (1st cycle)

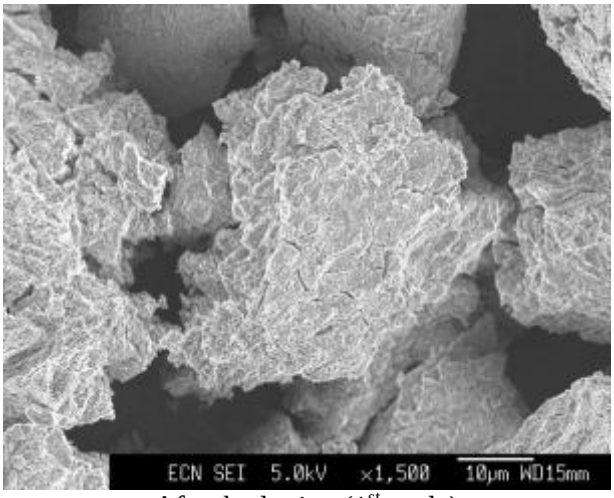

After hydration (1st cycle)

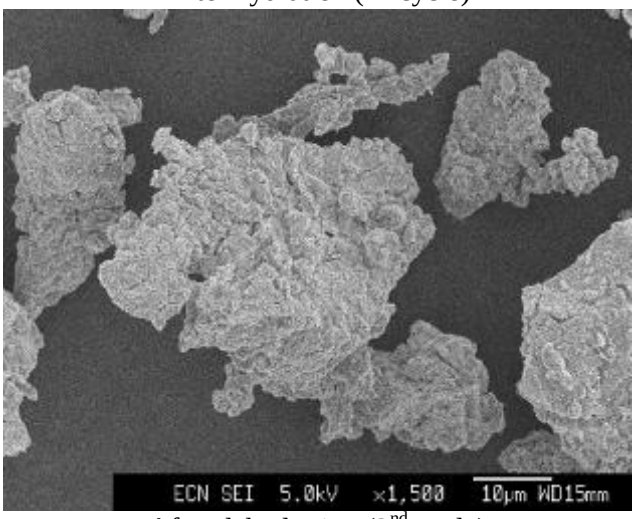

After dehydration (2nd cycle)

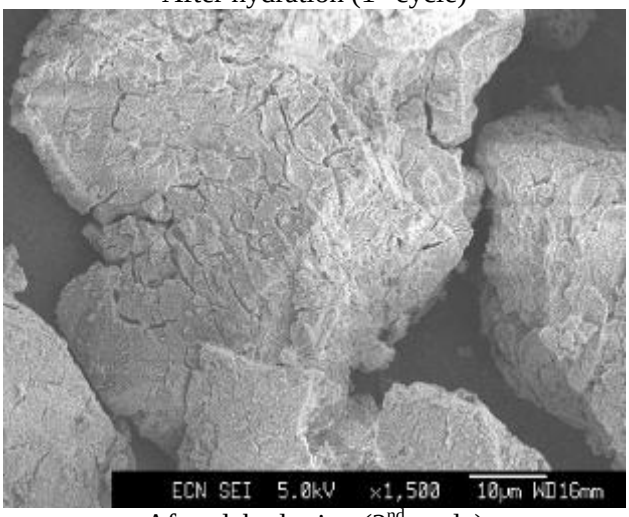

After dehydration (2nd cycle)

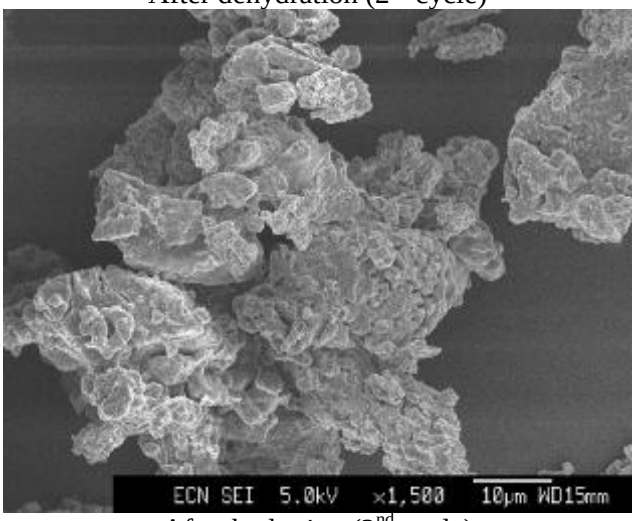

After hydration (2nd cycle)

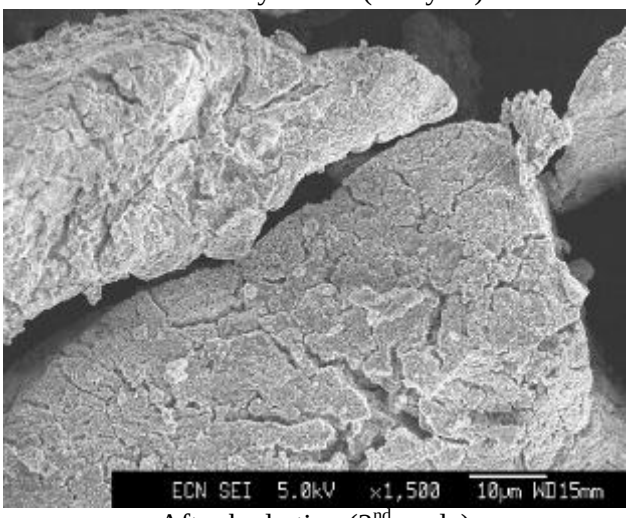

After hydration (2nd cycle)

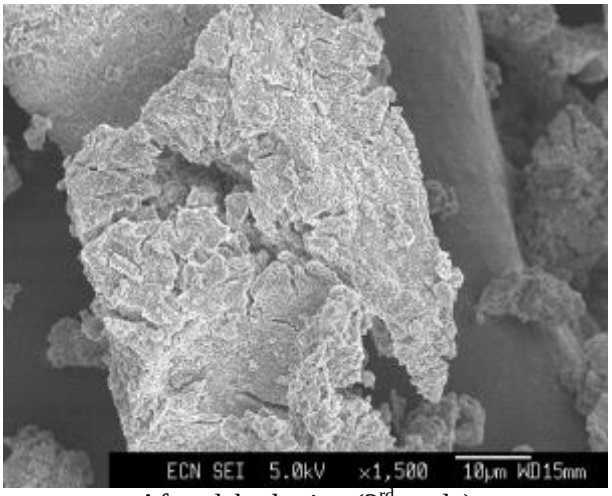

After dehydration (3rd cycle)

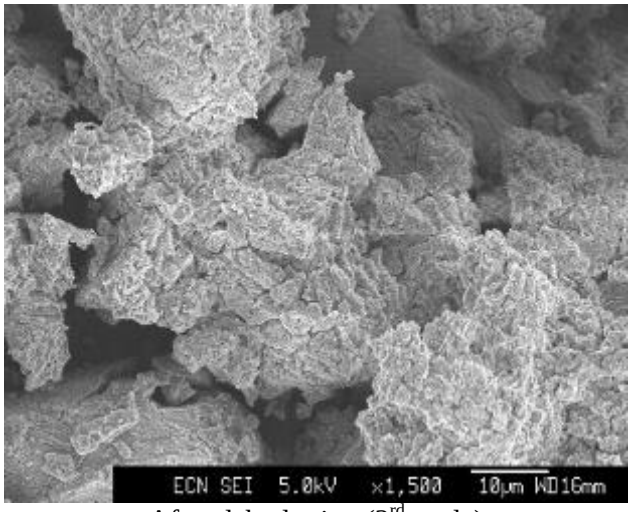

After dehydration (3rd cycle)

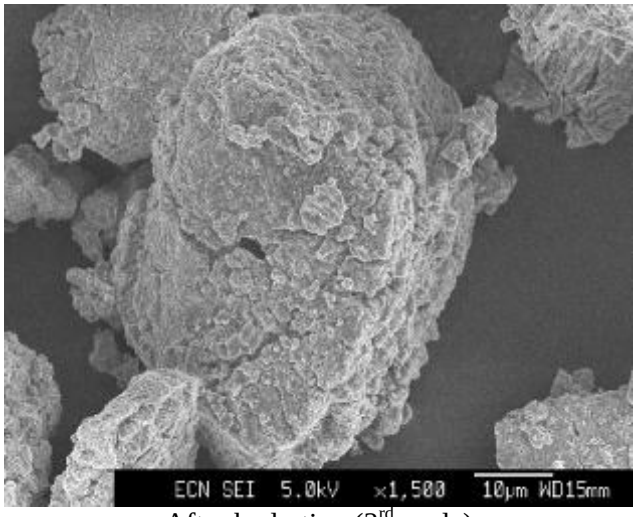

After hydration (3rd cycle)

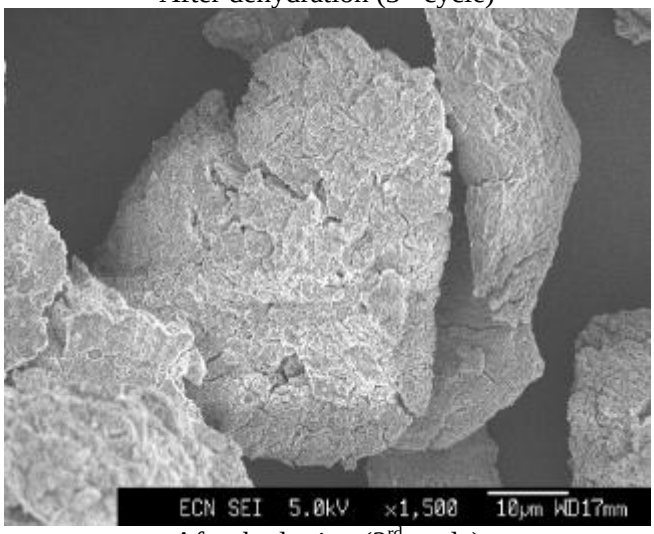

After hydration (3rd cycle)

# Appendix E results from porosity measurements after dehydration of the material

**Mercury intrusion porosimetry measurements for two samples: $MgSO_4.7H_2O$ from Merck and from VWR**

***Measurement conditions :***

- Apparatus used: Autopore III from Micromeritics
- Contact angle : 140 degrees
- Surface tension of Mercury (20°C) : 480 dynes/cm
- Mercury density (room temperature) : 13,5310 $g/cm^3$
- Volume of the penetrometer: 3,6404 ml
- Volume of the stem: 0,4120 ml

***Results :***

| | **$MgSO_4$ $7H_2O$ Merck** | **$MgSO_4$ $7H_2O$ Tu/e** |
|---|---|---|
| **Mass sample** | 0,1812 G | 0,1808 G |
| **Total volume of intrusion** | 0,1840 ml/g | 0,1906 ml/g |
| **Average diameter of the pores** | 0,9 µm | 0,6 µm |
| **Apparent density** | - | - |
| **Skeletal density** | - | - |
| **Porosity between particles** | 54,2 % | 54,5 % |
| **Porosity within particles** | 12,7 % | 14,1 % |

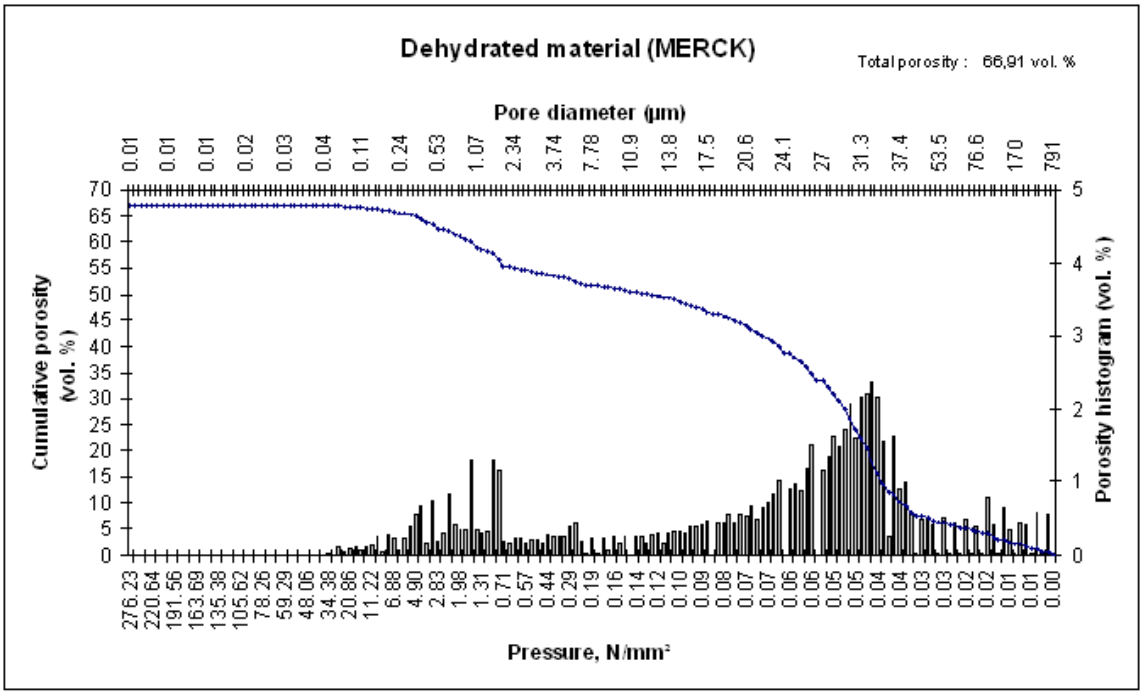
Dehydrated material (MERCK)
Total porosity : 66,91 vol. %
Pore diameter (µm)
0.01 0.01 0.01 0.02 0.03 0.04 0.11 0.24 0.53 1.07 2.34 3.74 7.78 10.9 13.8 17.5 20.6 24.1 27 31.3 37.4 53.5 76.6 170 791
Cumulative porosity (vol. %)
Porosity histogram (vol. %)
276.23 220.64 191.56 163.69 135.38 105.62 78.26 59.29 48.06 34.38 20.86 11.22 6.88 4.90 2.83 1.98 1.31 0.71 0.57 0.44 0.29 0.19 0.16 0.14 0.12 0.10 0.09 0.08 0.07 0.07 0.06 0.06 0.05 0.05 0.04 0.04 0.03 0.03 0.02 0.02 0.01 0.01 0.00
Pressure, N/mm²

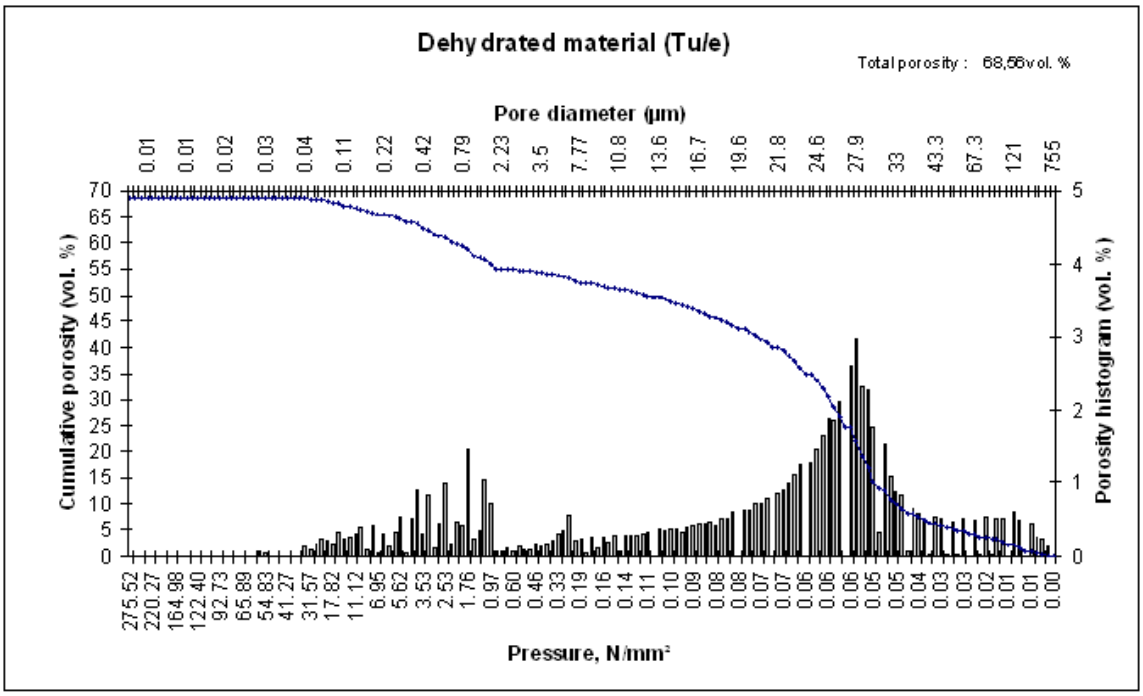
Dehydrated material (Tu/e)
Total porosity : 68,56vol. %
Pore diameter (µm)
0.01 0.01 0.02 0.03 0.04 0.11 0.22 0.42 0.79 2.23 3.5 7.77 10.8 13.6 16.7 19.6 21.8 24.6 27.9 33 43.3 67.3 121 755
Cumulative porosity (vol. %)
Porosity histogram (vol. %)
275.52 220.27 164.98 122.40 92.73 65.89 54.83 41.27 31.57 17.82 11.12 6.95 5.62 3.53 2.53 1.76 0.97 0.60 0.46 0.33 0.19 0.16 0.14 0.11 0.10 0.09 0.08 0.08 0.07 0.07 0.06 0.06 0.06 0.05 0.05 0.04 0.03 0.03 0.02 0.01 0.01 0.00
Pressure, N/mm²

# Appendix F Results from measurements performed by Netzsch Application Laboratory

F1. Material from Merck; $P_{H2O}$=1.3 kPa, Hydration temperature is 25°C

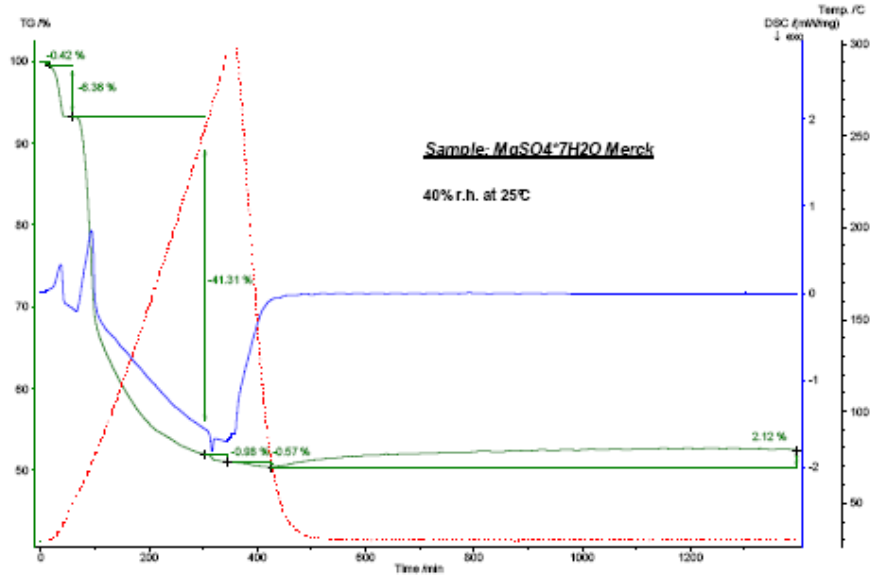


**Figure 1:** Mass changes (TG), heat flow rate (DSC) and temperature of the $MgSO_4 \cdot 7H_2O$ (Merck) sample measured at 40% r.h. at 25°C.

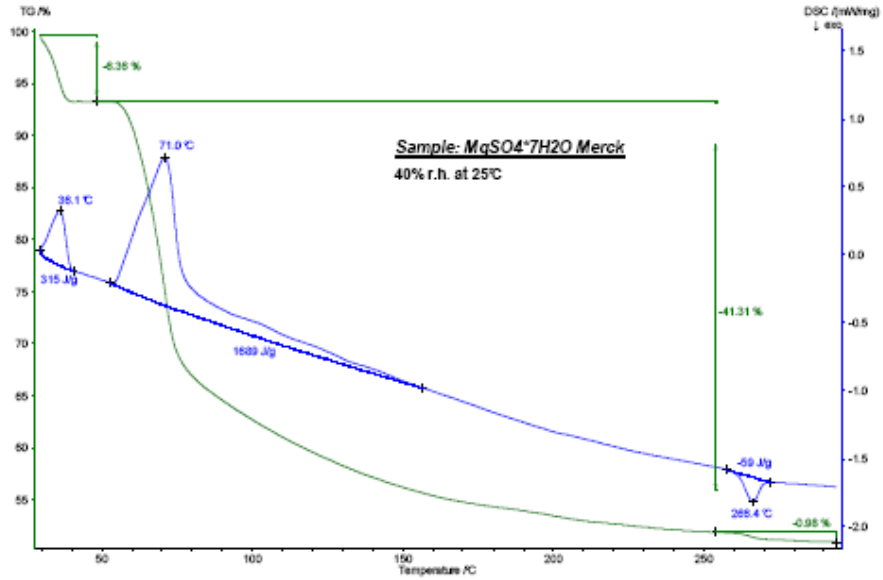


**Figure 2:** Temperature-dependent mass changes (TG) and heat flow rate (DSC) of the $MgSO_4 \cdot 7H_2O$ (Merck) sample measured at 40% r.h. at 25°C.

F2. Material from Merck; $P_{H2O}$=2.1 kPa, Hydration temperature is 25°C

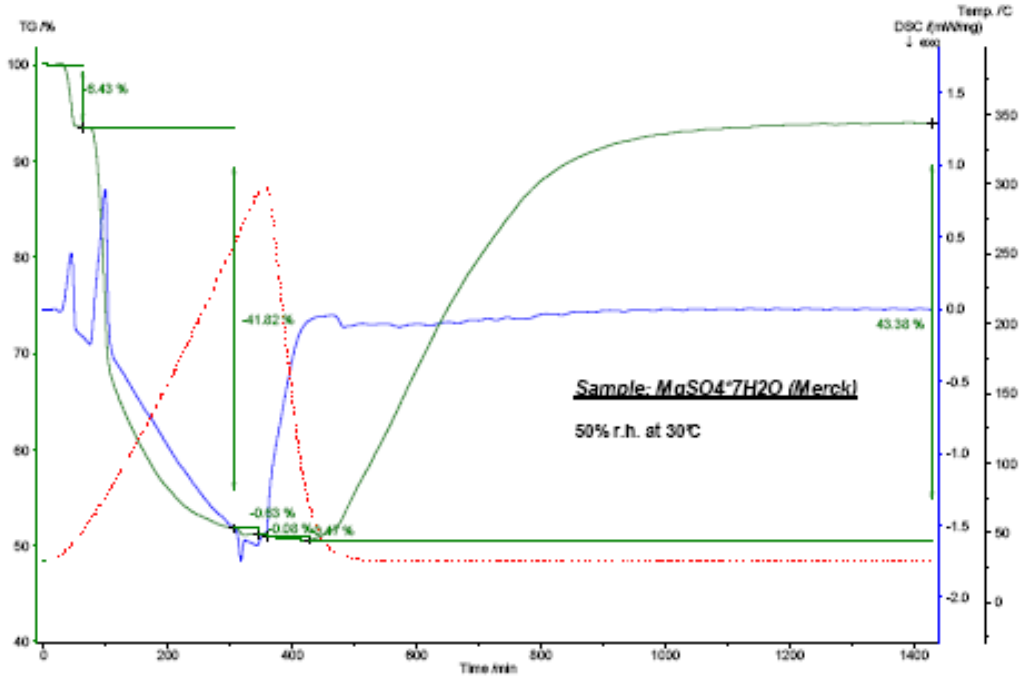


**Figure 3:** Mass changes (TG), heat flow rate (DSC) and temperature of the $MgSO_4 \cdot 7H_2O$ (Merck) sample measured at 50% r.h. at 30°C.

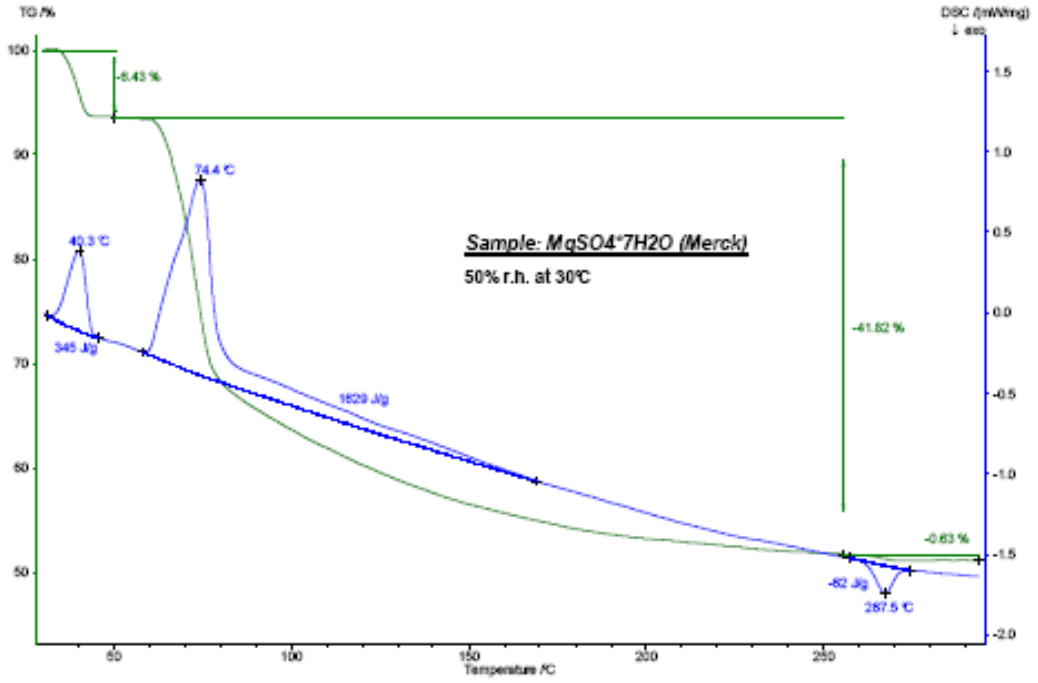


**Figure 4:** Temperature-dependent mass changes (TG) and heat flow rate (DSC) of the $MgSO_4 \cdot 7H_2O$ (Merck) sample measured at 50% r.h. at 30°C.

F3. Material from VWR; $P_{H2O}$=1.3 kPa, Hydration temperature is 25°C

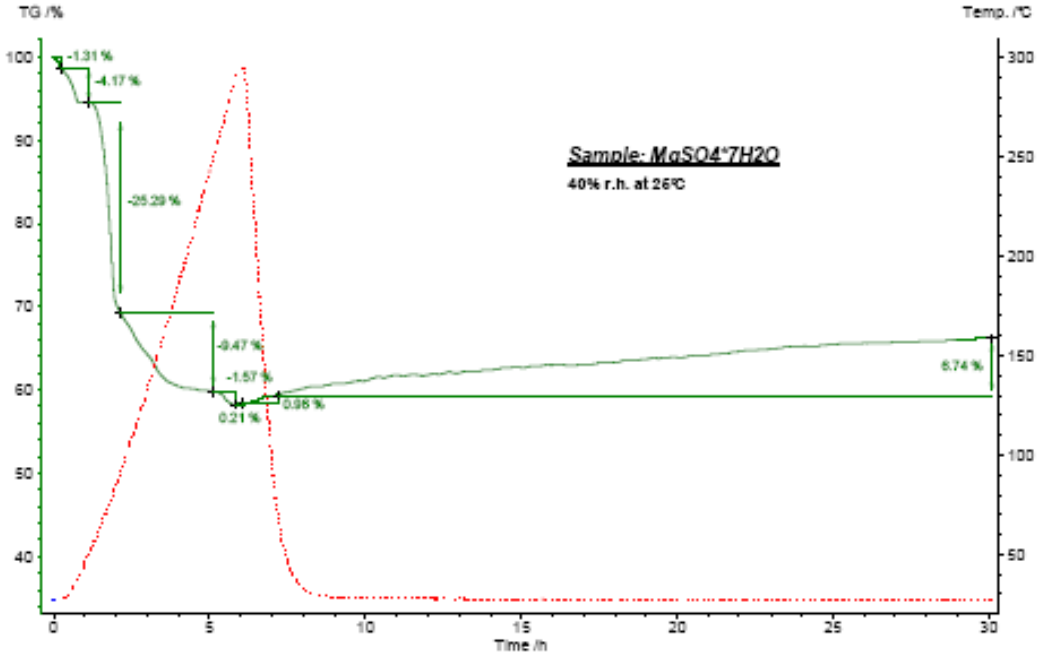


**Figure 1:** Mass changes (TG) and temperature of the $MgSO_4 \cdot 7H_2O$ sample measured at 40% r.h. at 25℃.

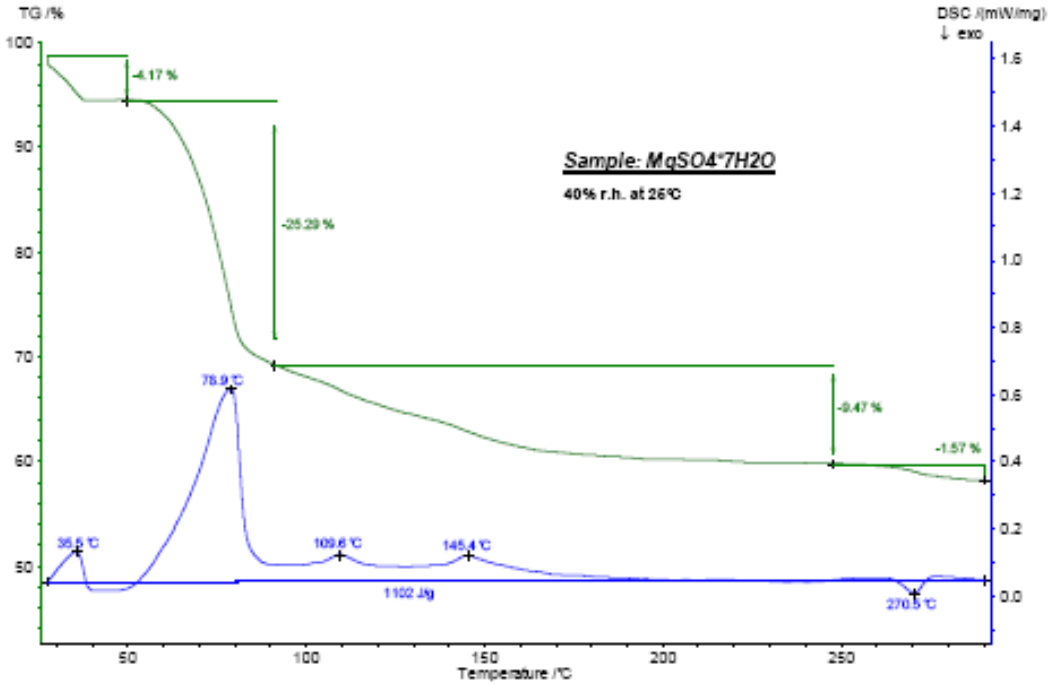


**Figure 2:** Temperature-dependent mass changes (TG) and heat flow rate (DSC) of the $MgSO_4 \cdot 7H_2O$ sample measured at 40% r.h. at 25℃.

F4. Material from VWR; $P_{H2O}$=2.1 kPa, Hydration temperature is 25°C

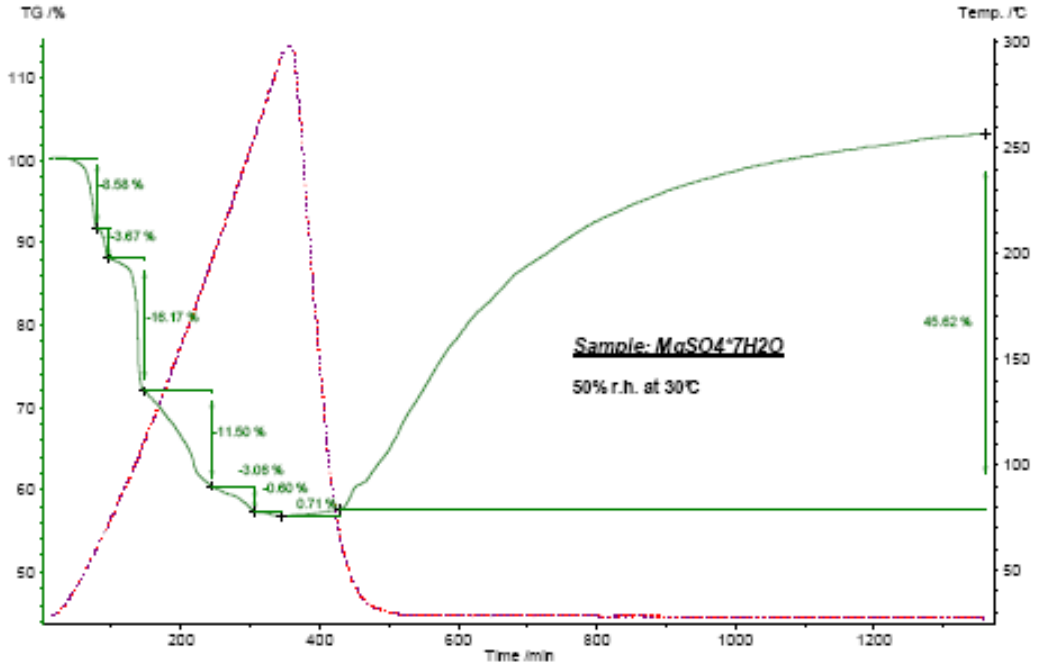


**Figure 3:** Mass changes (TG) and temperature of the $MgSO_4 \cdot 7H_2O$ sample measured at 50% r.h. at 30℃.

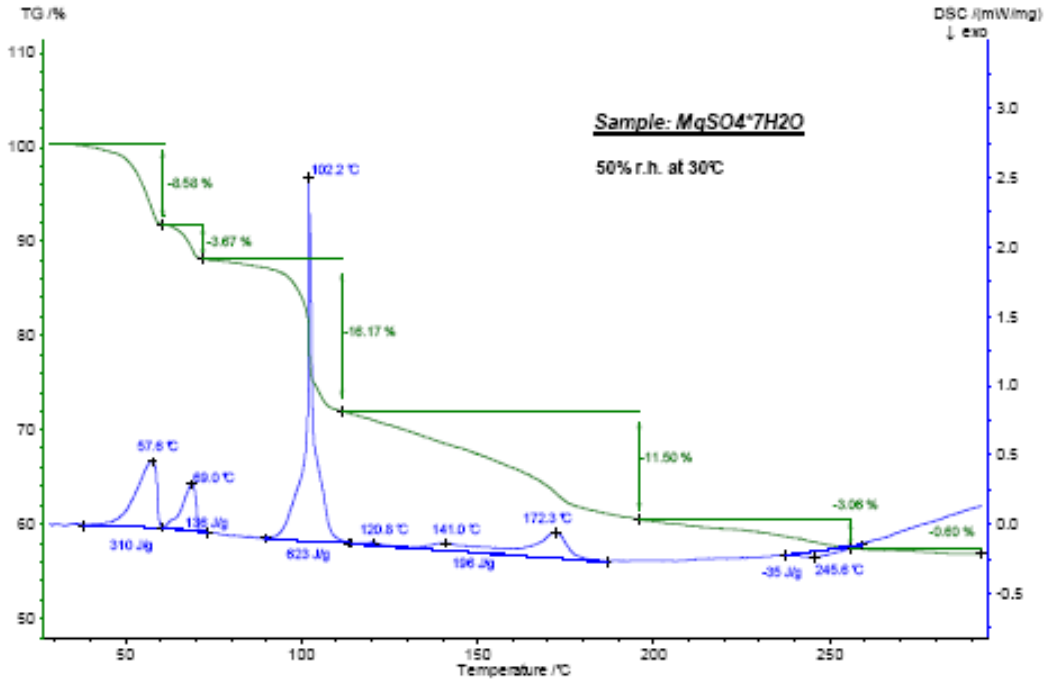


**Figure 4:** Temperature-dependent mass changes (TG) and heat flow rate (DSC) of the $MgSO_4 \cdot 7H_2O$ sample measured at 50% r.h. at 30℃.

B5. Material from VWR; $P_{H2O}$=2.1 kPa, Hydration temperature is 50°C

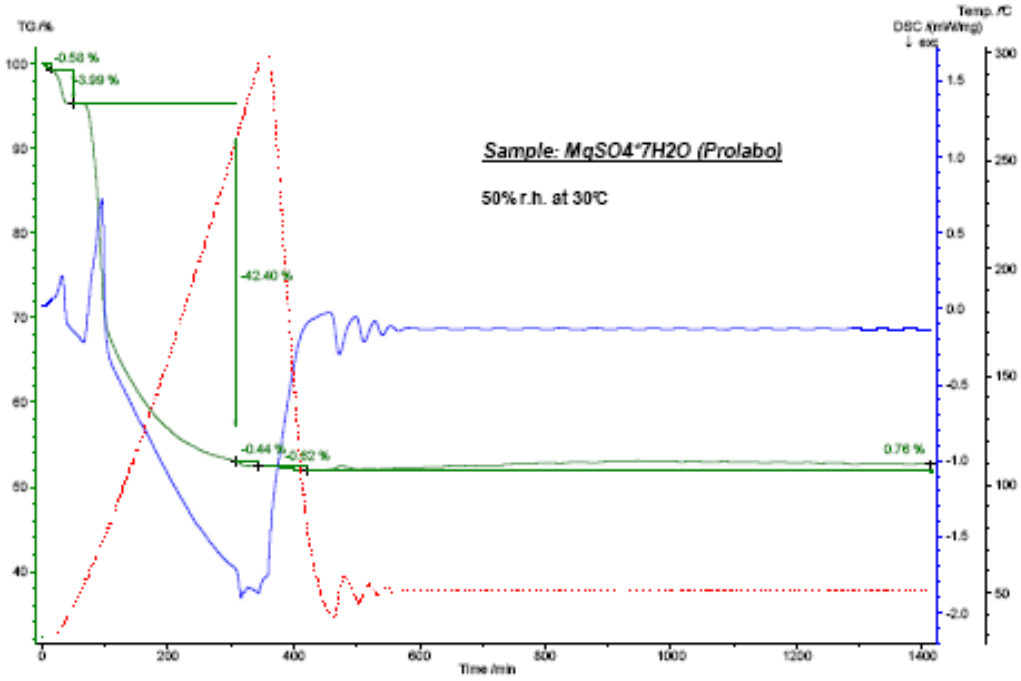


**Figure 5:** Mass changes (TG), heat flow rate (DSC) and temperature of the $MgSO_4 \cdot 7H_2O$ (Prolabo) sample measured at 50% r.h. at 30°C.

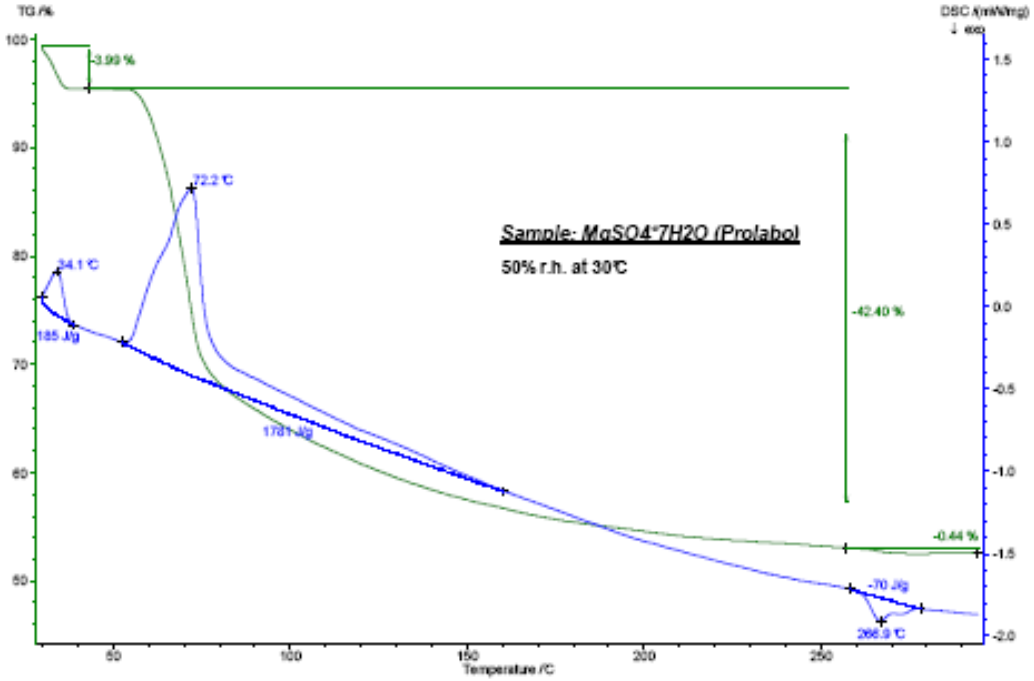


**Figure 6:** Temperature-dependent mass changes (TG) and heat flow rate (DSC) of the $MgSO_4 \cdot 7H_2O$ (Prolabo) sample measured at 50% r.h. at 30°C.